12-2018

Three Dimensional Carbon Nanotube Yarn Based Perovskite Solar Cells

Istiak Hussain
The University of Texas Rio Grande Valley

THREE DIMENSIONAL CARBON NANOTUBE YARN BASED PEROVSKITE SOLAR CELLS

A Thesis

by

ISTIAK HUSSAIN

Submitted to the Graduate College of
The University of Texas Rio Grande Valley
In partial fulfillment of the requirements for the degree of

MASTER OF SCIENCE

December 2018

Major Subject: Chemistry

THREE DIMENSIONAL CARBON NANOTUBE YARN BASED PEROVSKITE SOLAR CELLS

A Thesis
by
ISTIAK HUSSAIN

COMMITTEE MEMBERS

Dr. Mohammed Jasim Uddin
Chair of Committee

Dr. Elamin E. Ibrahim
Committee Member

Dr. Javier Macossay-Torres
Committee Member

Dr. Evangelia Kotsikorou
Committee Member

December 2018

ABSTRACT

Hussain, Istiak, Three Dimensional Carbon Nanotube Yarn Based Perovskite Solar Cells. Master of Science (MS), December, 2018, 61 pp., 29 figures, references, 117 titles.

Perovskite solar cells (PSC) have emerged as a promising photovoltaic technology in lab scale with a short time of research due to their high power conversion efficiency, simple device fabrication, all solid-state structure and the possibility to ingrate the traditional device into fiber format. In this work, a three-dimensional (3D) perovskite solar cell is demonstrated using functionalized carbon nanotube yarn (CNT) as both cathode and anode. TiO_2 and 2,2,7,-7-tetrakis(N,N-di-p-methoxyphenylamine)-9,9′-spirobifluorene (Spiro-OMeTAD) are used as the electron transporting and hole transporting material respectively. The TiO_2 oxide layer is deposited on the top of the twisted carbon nanotube yarn and annealed with $TiCl_4$ to get the uniform electron transport layer. A dip coating process is employed to produce a uniform perovskite layer on top of the TiO_2 oxide layer. Platinized carbon nanotube yarn is wrapped around on the top of the hole transporting layer and serves as the counter electrode. Under AM 1.5 100mWcm^{-2} illumination, a maximum power conversion efficiency (PCE) of 0.631% achieved with a high open current voltage (V_{OC}) of 0.825V. This three-dimensional all solid state perovskite solar cell shows a promising prospect in portable and wearable textile electronics.

DEDICATION

The completion of my master's studies would not have been possible without the love and support of my family. My mother SHAMIMA AKTAR, my father IQBAL HUSSAIN and my wife JAHURA FERDOUS, wholeheartedly inspired, motivated and supported me by all means to accomplish this degree. Thank you for your love and patience.

ACKNOWLEDGEMENTS

I will be always grateful to my advisor Dr. Mohammed Jasim Uddin for his invaluable supervision in scientific research and encouraging me with infinite patience and relentless positivity to complete my research work. I still remember when I first came to the University of Texas Rio Grande Valley, I was the only Bangladeshi student in Brownsville campus. From then, Dr. Uddin gave me his endless love, which helped me to grow up both in my research and personal characteristics. I am thankful to my dissertation committee members: Dr. Elamin E. Ibrahim, Dr. Javier Macossay-Torres and Dr. Evangelia Kotsikorou for their insightful advice and constructive comments on my graduate research and thesis. I am particularly thankful to Dr. Elamin E. Ibrahim for helping me with the FTIR measurement, and Dr. Ahmed Touhami for helping me with AFM characterization and Felipe for helping with SEM characterization. I would also like to thank the department chairs, Dr. Yuanbing Mao and Dr. Justin Moore and the graduate student coordinators, Dr. Evangelia Kotsikorou and Dr. Jason Parsons for making my time great in the graduate college of UTRGV. Much of this work would not have been possible without the help of my fellow graduate students Aminur Rashid Chowdhury and Jared Jaksik. I must thank Aminur Rashid Chowdhury for his all means of support during the experiment and writing my dissertation. I enjoyed discussing scientific research with him. I still remember the night how we were excited when we successfully developed the solar cell. I would like to thank Jared Jaksik for reviewing my thesis. I feel fortunate to meet Dr. Phong Tran and thank to him for getting me started and setting me on the right path. Finally but most importantly, I would like

to thank my beloved parents for their unconditional love and support in my whole graduate journey and my wife for supporting me mentally and showing great understanding during my graduate research.

TABLE OF CONTENTS

Page

LIST OF FIGURES

Page

CHAPTER I

INTRODUCTION

The energy crisis has become a global issue these days. At present, most of the world's energy is consumed by non-renewable sources. According to US Energy Administration (EIA), 81% of the energy consumed by fossil fuels such as coal, petroleum and natural gas, while only 10% of energy consumed by renewable energy and rest of 9% of the energy is consumed by nuclear power electric (Figure 1) [1]. In addition, in 2016, 64% of electricity was generated from fossil fuels, and 20% was generated from nuclear energy sources, while only 15% was from renewable energy sources (Figure) [2]. However, the demand for renewable energy is ever increasing due to the depletion of fossil fuels and the growing concerns about climate change and global warming [3]. Among different renewable sources, solar energy technology is most promising technologies to fulfill the world's energy demand, and it has seen the most consumer availability and widespread utilization, where other sources like wind, geothermal, hydroelectric power generation require specific environmental conditions to be feasible [4,5]. The world receives more energy from the sun in one hour than the world's yearly energy demand [6]. Although only 1% of the world's energy production was reported to be solar-driven in 2013, solar energy is projected to become the largest source of energy by 2050 [5]. Perovskite solar cell is a device that converts the energy of incident photons directly to electricity [7]. The development of photovoltaic solar cells can be classified into three discrete generation such as

first generation (1G), second generation (2G) and third generation (3D). 1G solar cells are developed based on silicon wafers which can exhibit high efficiency. However, it has high production costs. With the aim to reduce the production costs, 2G solar cells were developed, which are commonly based on amorphous silicon, copper indium gallium selenide (CIGS), and cadmium telluride (CdTe). However, the overall performance of 2G solar cells was not promising compared to their 1G counterparts, which has prompted the development of 3G or emerging solar cell technologies [8]. 3D solar cells include copper / zinc / tin sulfide solar cells, dye-sensitized solar cells, organic solar cells, polymer solar cells, perovskite solar cells are aimed to developed to increase efficiencies with maintaining the economic and environmental cost advantages of thin film deposition techniques [9]. Figure 3 shows the efficiency and cost projection of three photovoltaic generations.

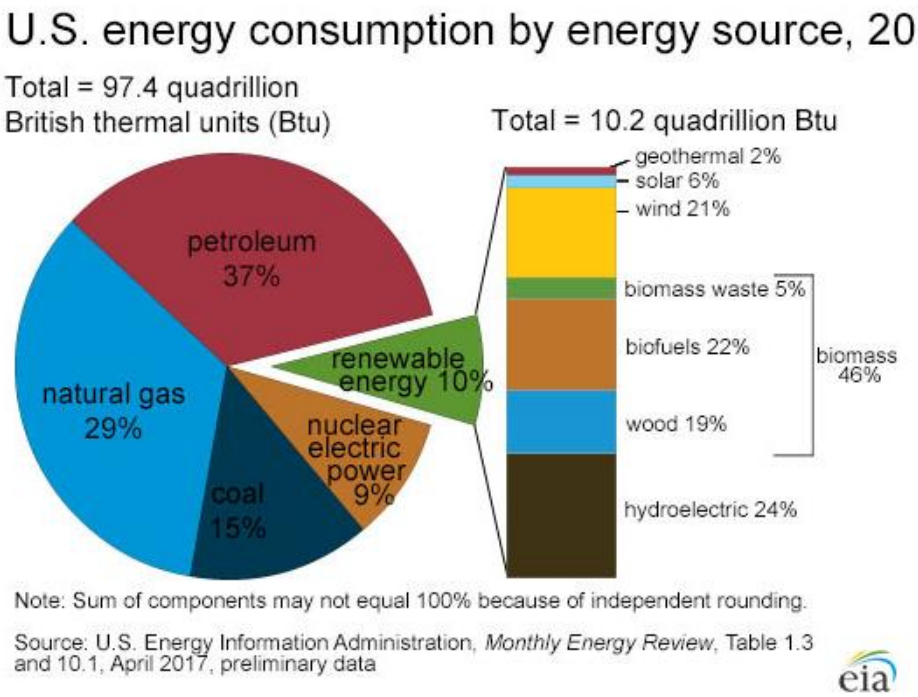

Figure 1: US Energy Consumption by Energy Source [10].

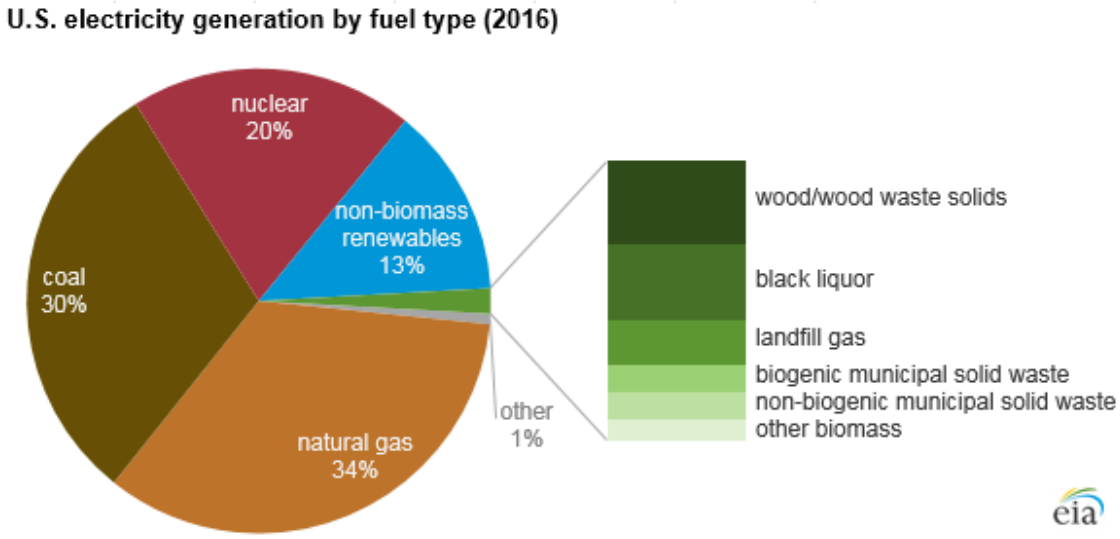

Figure 2: US Electricity Generation by Fuel Sources [11].

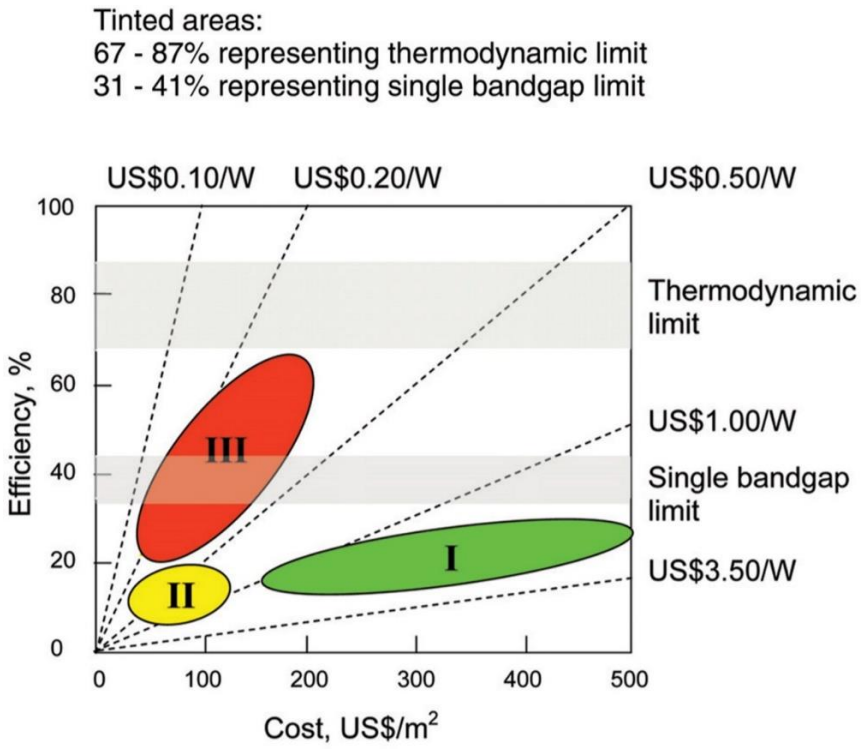

Figure 3: Efficiency and cost projection of the first, second and third generation photovoltaic solar cells [9].

Among different 3G photovoltaic solar cells, perovskite solar cells are the most promising technology regarding research and development. Perovskite solar cells were originated from dye-sensitized solar cells in 2009. PSC was first introduced in the literature in 2009 with a power conversion efficiency of 3.8% [12]. Kojima *et al.* first utilized CH3NH3PbI3 (methylammonium lead iodide or MAPbI3) and CH3NH3PbBr3 (methylammonium lead bromide or MAPbBr3) as a light sensitizer in a liquid electrolyte based dye-sensitized solar cell (DSSC) architecture [12]. However, due to the device stability issues and the instant dissolution of perovskite material in a liquid electrolyte during operation, it did not receive much attention until 2012. The interest in PSCs was triggered when Kim et al. developed a solid state, high efficient and stable PSC in 2012 by replacing the liquid electrolyte with the solid hole conductor [13]. After that, perovskite solar cells have been intensively studied in the past few years because of some unique properties of perovskite materials such as high absorption coefficient [14], tunable bandgap [15], long charge carrier (electron-hole) diffusion lengths [11], and low-temperature solution processability [17]. In addition, the efforts to design the novel device architectures [18,19], optimization of interfacial characteristics [20,21], compositional engineering of perovskite materials [22], and careful control of the morphology of each functional layer [23,24] have improved the performance of PSCs. These advantages and advances have attracted scientific community a great interest. Consequently, there is a tremendous increase in the number of publications (Figure 4). In accordance with these research trends, PSCs reached a maximum power conversion efficiency of 23.7% from 3.8% over the previous nine years (Figure 5).

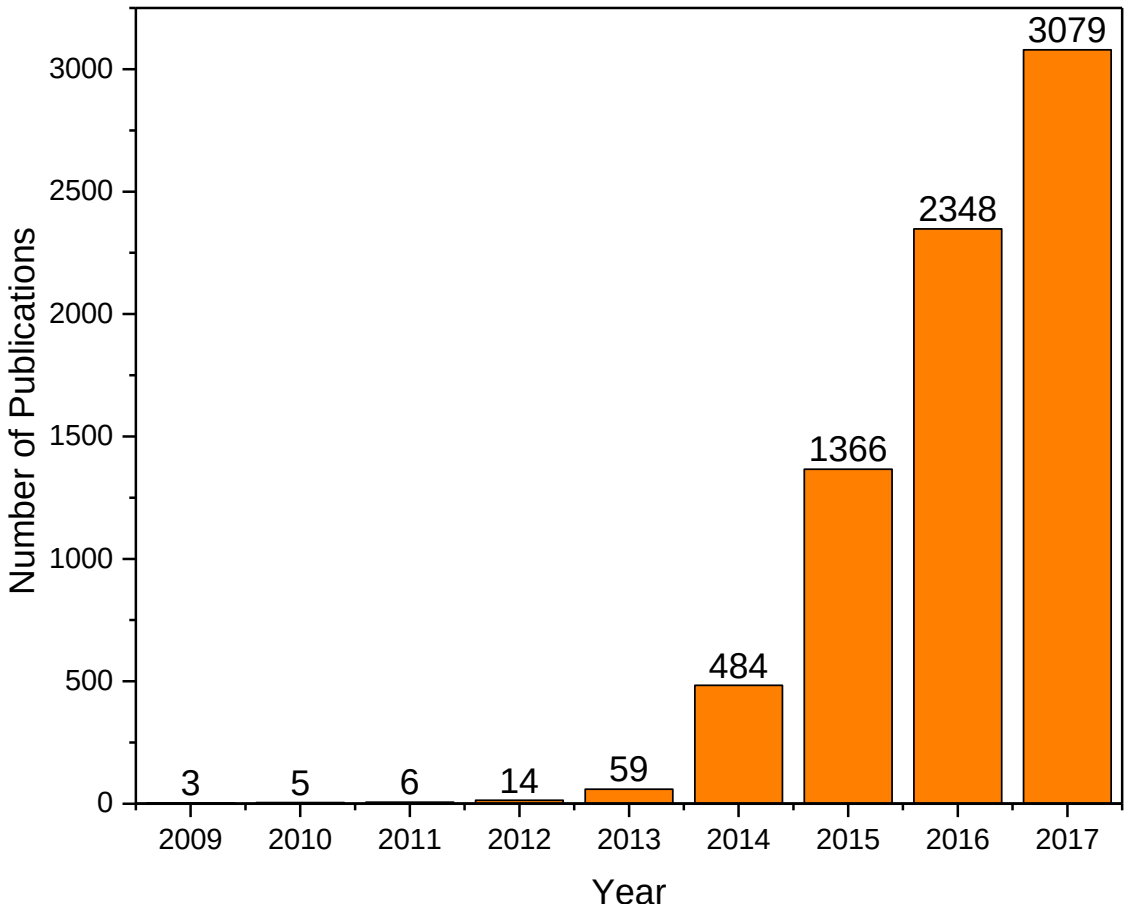

Figure 4: Research trends in perovskite solar cell based on the number of published articles (data source ISI Web of Knowledge).

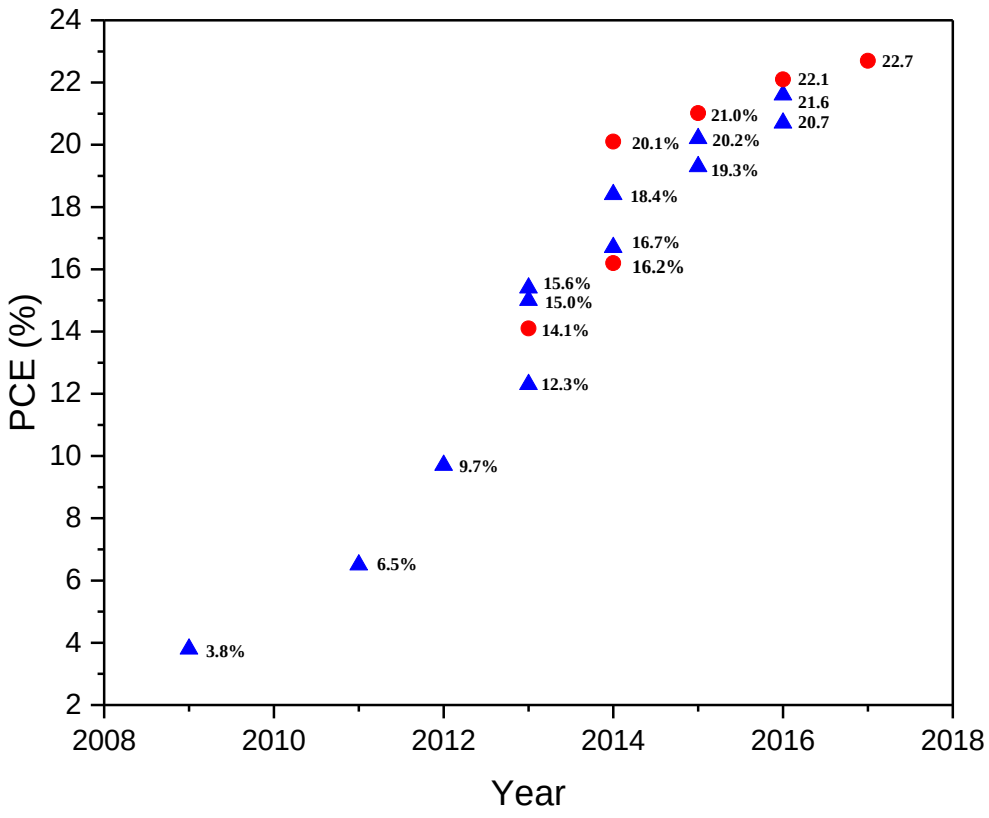

Figure 5: The progress in PCE of PSCs: 3.8% [12], 6.5% [25], 9.7% [13], 10.9% [26], 12.3% [27], 15.0% [28], 15.4% [29], 16.7% [30], 18.4% [31], 19.3% [32], 20.2% [33], 20.7% [34], and 21.6% [35]. Values in red represent certified efficiencies [36].

The materials used in different functional layer of perovskite solar cells can be categorized into five different groups: the working electrode – typically transparent conductive oxide (TCO) layer, the electron transporting layer (ETL), the light absorbing / harvesting perovskite layer, the hole transporting layer (HTL) and the counter electrode – typically metal contact material. The conventional PSCs utilized flat cell design which requires a (TCO) usually – fluorine-doped tin oxide (FTO) or indium tin oxide (ITO) coated glass substrates. However,

transparent conductive oxide has several drawbacks. These glass substrates are expensive as well as their rigidity, weight, and frangibility limit the integration of PSCs into portable and wearable electronics [37,38]. The working/counter electrode materials used in solar cells have a significant impact on the overall efficiency of the device. The working electrode should have a good surface to be well coated with the oxide material and have the high conductivity to allow the transportation of the photo-generated electron with minimal resistance. Ti wire and stainless steel have already been used in perovskite solar cells as working electrode [39,40]. Carbon nanotube yarn is a promising material that has the potentiality to use in the three-dimensional solar cell as electrode materials, which allow facile chemical functionalization, good conductivity and more flexible than metallic wires [41–43].

In summary, the objective of this research was to develop flexible, three dimensional, solid-state perovskite solar cells utilizing carbon nanotube as both working and counter electrode. The methodology used for the fabrication of PSCs was fully solution based and integrated the conventional PSCs configuration into a three-dimensional format. Finally, the morphological characterization of each functional layer and electrical characterization of the three-dimensional cells were carried out.

CHAPTER II

LITERATURE REVIEW

Fundamentals of Solar Cells

The working mechanism of the solar cell is based on the photovoltaic effect which is the generation of a potential difference at the junction of two different materials in response to the electromagnetic radiation. The photovoltaic effect occurs when a semiconducting material is illuminated by light with photons of equal or higher energy than the semiconducting material energy gap. The energy gap of semiconducting material is the energy difference between the top of the valence band (energy level for electrons farthest away from the atom nucleus) and bottom of the conduction band (energy level required for electrons to be excited to make the material conductive). The energy gap can also be described as the energy difference between the highest occupied molecular orbital (HOMO) and the lowest unoccupied molecular orbital (LUMO). If the photon contains energy higher than the semiconducting material, it can be absorbed and promote an electron from the valence band/HOMO to the conduction band/LUMO. Consequently, a vacancy is created in the valence band, which is called hole. Electron-hole pairs are formed by combing together the electrons and hole in the conduction band and valence band respectively. The exciton diffusion to the donor-acceptor interface where exciton dissociates into free charge carriers after overcoming the binding energies. The free charge carriers (electrons and holes) transport to the respective electrodes (working and counter) under the internal electric

fields, and then generate photocurrent and voltage.

Operation Principle of Perovskite Solar Cell

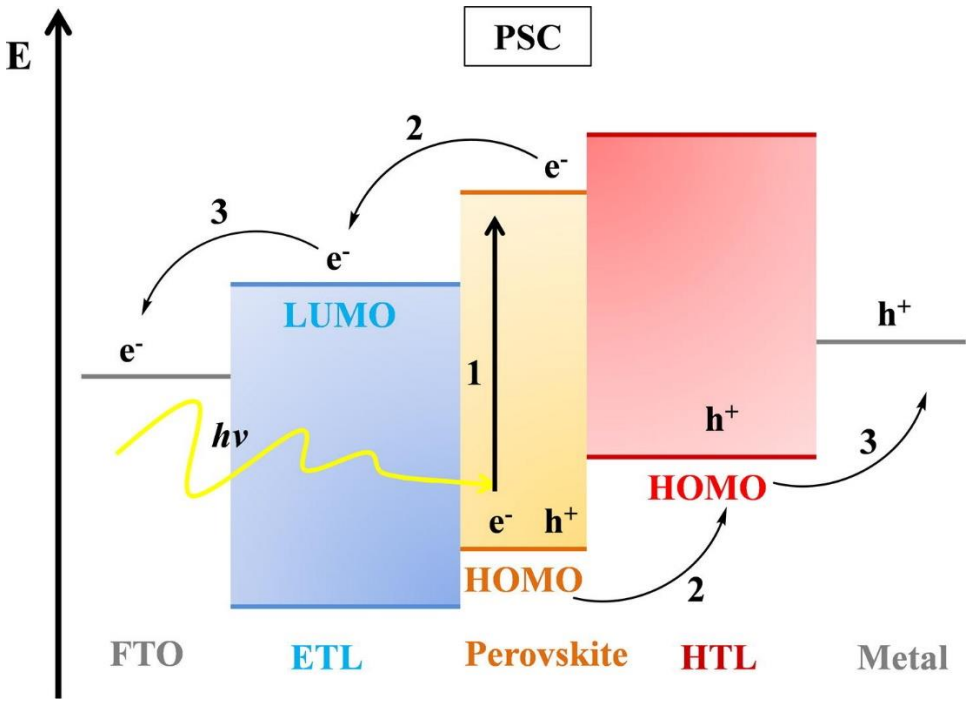

Figure 6: Operational mechanism of a perovskite solar cell [44].

A schematic diagram of the operation mechanism of perovskite solar cells is illustrated in Figure 6. The photovoltaic system in PSCs can be described into three different steps: (1) absorption of photons followed by free charge (electron and hole) generation (2) charge transportation and (3) charge extraction. When sunlight hits on PSCs, the active perovskite layer absorb the light (photons), excitons are generated if the energy of the photon is higher than the energy gap of the perovskite material. The internal potential created from the work function difference between the working electrode and counter electrode allows the excitons to be separated to free charge carriers [45]. The free charge carriers are produced upon exciton dissociation which occurs at the interface between the active perovskite layer and charges

transporting layer. When the electrons are separated from the holes, they are transported to the electron transporting layer followed by migrating to the working electrode. Simultaneously, the holes are transported to the hole-transporting layer and then migrates to the counter electrode. Working and counter electrodes collect the electrons and holes respectively. Finally, an external load can be powered by connecting a circuit through it to produce photocurrent [46].

Photovoltaic Characterization Parameters

The parameters that are used to characterize the performance of a solar cell are: short-circuit current density J_{SC}, open circuit voltage V_{OC}, fill factor and power conversion efficiency. The first three parameters are determined from the J-V characteristics curve, however, fill factor can also be calculated the Jsc and Voc values. The power conversion efficiency can be determined from these three parameters. These parameters are very important in solar cell characterization as they determine how efficient the cell they can be optimized for designing efficient solar cell.

The short circuit current I_{SC} is defined as the current that flows through the external circuit when the two electrodes of the solar cells are short-circuited (i.e., when the voltage across the cell is zero). I_{SC} depends on the incident photon flux on the cell, which can be determined by the spectrum of the incident light. I_{SC} also depends on the active area of the cell. To remove the dependence of the cell area, instead of short circuit current the short circuit current density Jsc (mA/cm^2) is used which describe the maximum current delivered by a solar cell.

The open-circuit voltage V_{OC} is defined as the maximum voltage from the solar cell when the there is no current flow through the external circuit (i.e., when the cell terminals are open or

not connected to a load). Voc depends on the photo-generated current density and saturation current.

Fill factor is defined as the ratio between the maximum power generated by a solar cell to the products of the open circuit voltage (V_{OC}) and short circuit current (J_{SC}) of that cell. Mathematically fill factor can be expressed as:

$$FF = \frac{P_{\max}}{V_{OC} J_{SC}} = \frac{V_{MP} J_{MP}}{V_{OC} J_{SC}}$$

Where J_{MP} is the current density maximum power, and V_{MP} is the voltage at maximum power.

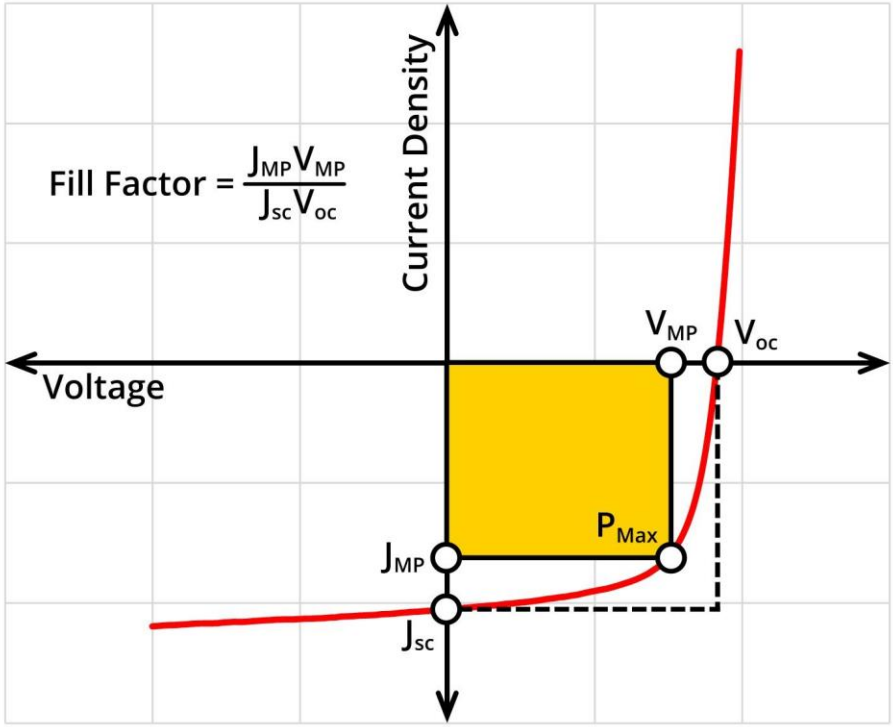

Figure 7: Typical J-V curve of a solar cell [47].

Power conversion efficiency is defined as the ratio between the maximum generated power and the incident power. Mathematically power conversion efficiency can be expressed as:

$$PCE = \frac{P_{\max}}{P_{in}} = \frac{J_{SC} V_{OC} FF}{P_{in}}$$

Where, P_{max} is the maximum power generated by a solar cell and P_{in} is total power of sunlight illuminated on the cell.

Perovskite Crystal Structure

The term 'perovskite' refers to a material with a particular crystal structure, is one of the most promising lights harvesting solar cell materials for next-generation solar cells. It was discovered in 1839 in the Ural Mountains in Russia and then named after Russian mineralogist L. A. Perovski [48]. While perovskite was initially referred to the mineral $CaTiO_3$ (calcium titanium oxide), compounds that have a similar crystal structure to $CaTiO_3$ (ABX_3) are also called perovskites (Figure 8). Generally, in the structure of ABX_3, A represents a large monovalent cation such as $CH_3NH_3^+$ (MA), $HC(NH_2)_2$ (FA) or Cs^+ which occupies the cubooctahedral site in a cubic space. B represents a small divalent metal cation such as Pb^{2+} or Sn^{2+} occupying the octahedral sites, and X is an anion, typically a halogen (Br, Cl, I), however, it could be oxygen, carbon or nitrogen. When halogen is used as an anion, A and B are usually monovalent and divalent cations respectively [49]. However, when O^{2-} is used, A and B are divalent and tetravalent respectively [49].

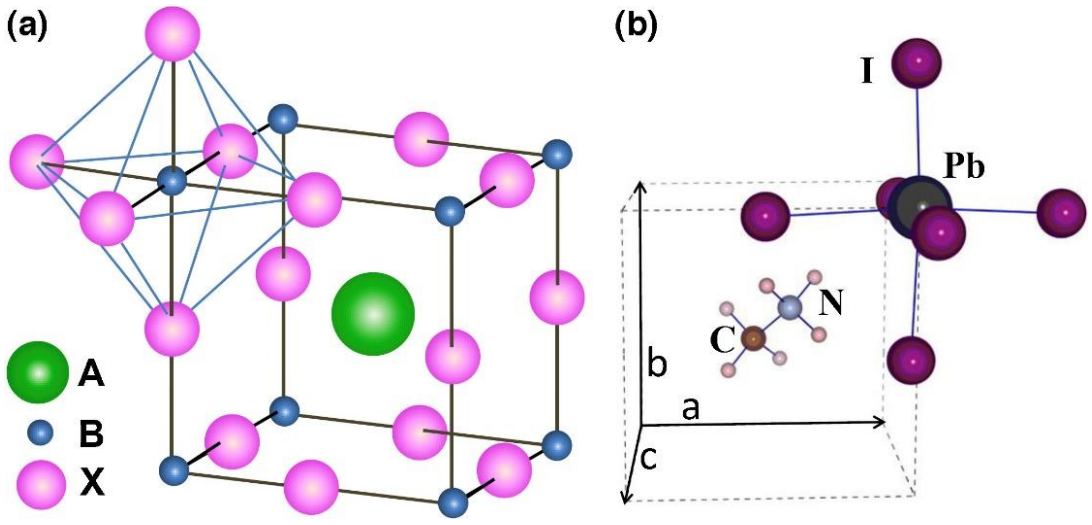

Figure 8: Crystal structure of perovskite (a) ABX_3 perovskite crystal structure showing BX_6 octahedral and large cation A occupied in the cubooctahedral site. (b) The unit cell of cubic $MAPbI_3$ perovskite [49].

The geometric tolerance factor and octahedral factor are two crucial parameters to quantify the structure and stability of the perovskite material. The tolerance factor, also called Goldsmith tolerance factor is expressed as the ratio of the bond lengths of A-X and B-X in an idealized solid-sphere model:

$$t = \frac{(R_A + R_X)}{\sqrt{2}(R_B + R_X)}$$

In the above equation, R_A, R_B, and R_X represent the effective ionic radii of the constituent ions A, B, and X respectively [50]. The octahedral factor is defined as the ratio of the ionic radii of the divalent cation (R_B) and anion (R_X). The tolerance and octahedral factor for halide perovskite are typically in the following range: $0.81 < t < 1.11$ and $0.44 < \mu < 0.90$ [51]. If the tolerance factor falls out of this range, the formation of 3D perovskite will be energetically unfavorable [51]. While t=1 gives a stable 3D cubic phase, the perovskite material still can hold

their stable 3D cubic structure with $0.89 \leq t \leq 1$ [51]. The calculated values of tolerance and octahedral factor of a set of 12 different perovskite material are shown in Figure 9.

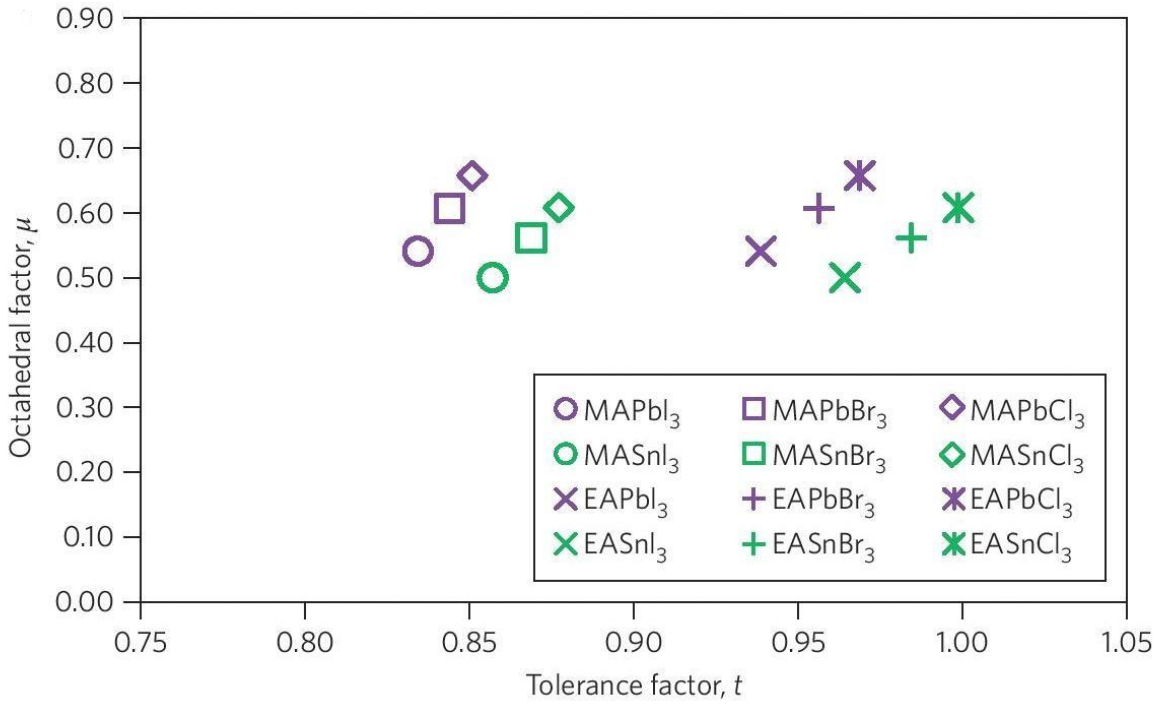

Figure 9: Calculated values of tolerance and octahedral factor for 12 different halide perovskite material [50].

Device Architecture

The architecture of perovskite solar cells can be categorized as either regular (n-i-p) or inverted (p-i-n) structure depending on which charge transport material (electron or hole) is encountered by the incident light first. The regular and inverted PSCs can be further classified as mesoscopic and planar structure. Charge transport layer free perovskite solar cells were also utilized such as electron transporting layer free and hole transporting layer free PSCs. In sum, six

different types of PSCs architectural design were evaluated by different researchers till now: such as mesoscopic n-i-p, planar n-i-p, mesoscopic p-i-n, planar p-i-n, ETL-free, and HTL-free architecture.

The regular n-i-p mesoscopic configuration was the very first arrangement of PSCs (Figure 10a). The assembly begins with a transparent conductive oxide (TCO) glass substrate usually FTO, followed by the electron transporting layer (ETL). The structure is then layered with a mesoporous metal oxide containing the light absorbing perovskite material followed by the hole transporting material usually spiro-OMeTAD. Finally, the device is capped with a metallic anode. The advancement of mesoporous PSCs led the photovoltaic researchers to the development of other PSC device configurations. Planar structure is the second arrangement of the PSCs, which is also the evolution of the mesoscopic PSC structure (Figure 10b). In the planar structure, the light harvesting perovskite payer is sandwiched between the electron transporting layer and hole transporting layer and it does not contain a mesoporous metal oxide layer, therefore, provide an overall simpler structure. Moreover, high power conversion efficiency can be achieved without the mesoporous layer by carefully controlling the interfaces between the different functional layers [32]. Using the same functional materials and approach, planar n-i-p PSC exhibited increased open circuit voltage (Voc) and short-circuit current density (J_{SC}) compared to a mesoscopic PSC device [52]. However, the planar PSC device had more severe J-V hysteresis than the mesoscopic PSC [52]. The grain and thickness of the active layer of planar PSC could influence the J-V hysteresis behavior [53,54]. The J-V hysteresis behavior also depends on the p-type hole transporting material that is used to construct the cell [55]. It is also found that this behavior can become negligible with a reduced capacitance which can be attributed by replacing spiro-OMeTAD with Poly(3,4-ethylene dioxythiophene)-poly(styrene

sulfonate) (PEDOT:PSS) or any other inorganic hole transporting materials [55]. In addition, the J-V hysteresis behavior is also dependent on the scan rate, scan direction, and range during the electrical characterization of the cell [56]. In general, the mesoporous PSC better efficiency than planar PSC, however a thinner mesoporous layer (less than 300nm) is required [25]. On the other hand, the planar PSC have low-temperature fabrication processability unlike the mesoporous PSC structure [57].

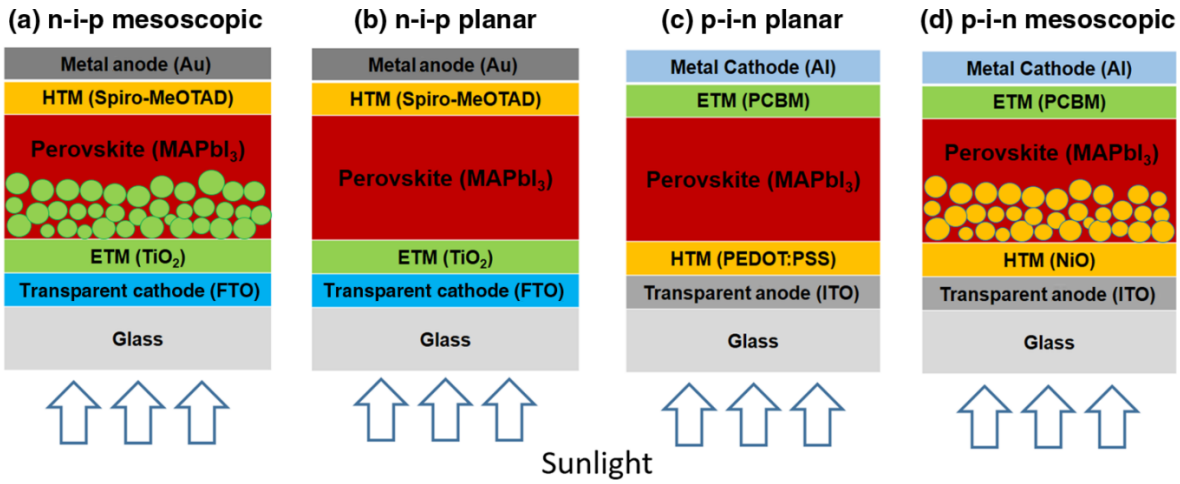

Figure 10. Schematic diagram of the four typical perovskite solar cells (a) n-i-p mesoscopic (b) n-i-p planar (c) p-i-n planar and (d) p-i-n mesoscopic [52].

The planar p-i-n structure is originated from the organic solar cell structure [58]. In the inverted planar structure, the hole transporting layer is deposited first wherein the regular structure the electron transporting layer is deposited first. Jeng *et al.* developed the first planar hetero-junction PSC with an inverted design configuration [59]. With the advancement in perovskite solar cells research, the inverted planar structure expanded the options to explore organic and inorganic materials for the selective layer of the cells [44]. Moreover, the planar p-i-n configuration allows the low-temperature fabrication process and show negligible hysteresis with enhanced efficiency. On the other hand, the mesoscopic p-i-n device allows using oxide

materials as the hole transporting layer to construct the cell [52]. The device configuration of inverted planar and mesoscopic PSC is shown in Figure 10c-d.

A compact n-type metal oxide on the transparent conductive oxide (TCO) is a requirement for conventional planar PSCs to achieve the high open circuit voltage (Voc) and therefore, high overall efficiency. Liu *et al*. developed an electron transport layer PSC by direct depositing the active perovskite layer on the indium oxide (ITO) through a sequential layer deposition method and exhibited a high PCE of 13.5% [60]. This development demonstrates that the inclusion of ETL is not necessary to obtain high efficiency [60]. Ke *et al.* also developed an electron transporting layer free PSC on the FTO substrate via a one-step solution process which showed a PCE of 14.4% with a high open current voltage of 1.06V [61]. The electron transporting layer free perovskite solar cell is shown in Figure 11.

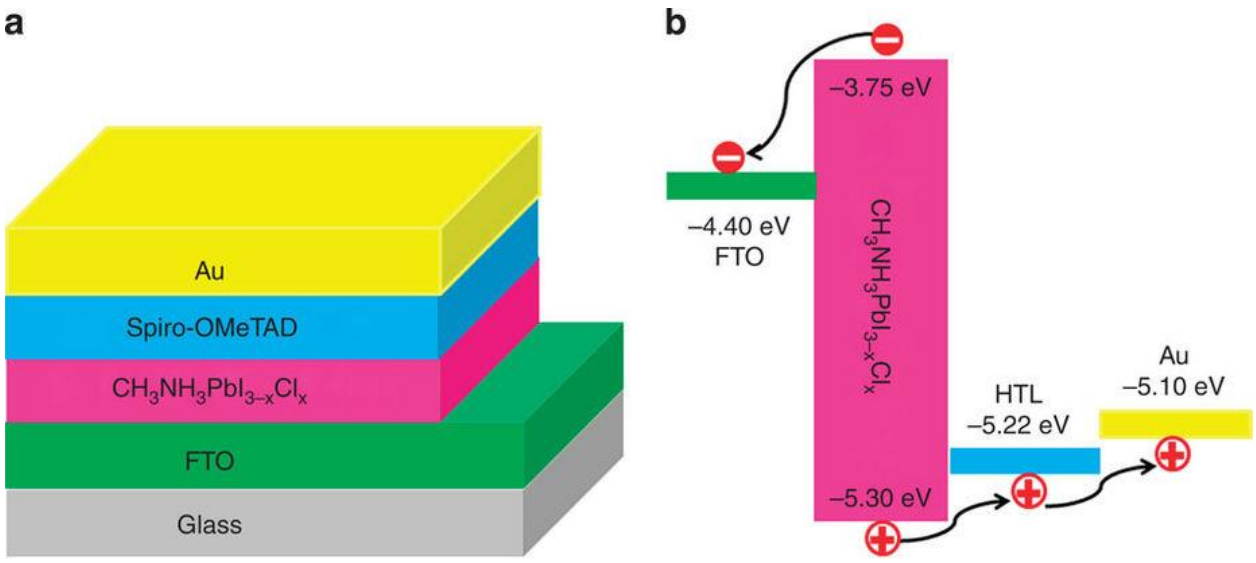

Figure 11: Schematic diagram of the electron transport layer free planar mixed halide perovskite solar cell (a) structure and (b) energy level diagram of the planar PSC showing collection and separation of photo-generated electrons and holes without an ETL [61]

Various novel hole-transporting materials including small molecules, polymer, and inorganic compounds have been used in PSC and exhibited excellent results. However, hole transporting free PSCs are garnering increasing attention in this field. The increased attention is because the high efficient PSCs contain expensive HTMs. Lead halide perovskite shows excellent semiconducting properties like long charge transport lifetimes and ambipolar nature which permits the exclusion of the hole transporting layer in PSCs [14,16]. Etgar *et al.* developed HTL-free PSC for the first time demonstrating that perovskite itself can perform the role of both light harvester and hole conductor [62]. Aharon *et al.* found that the depletion layer has a significant influence on the performance of HTL-free PSCs as this layer aids in charge separation and inhibits the back reaction of the electrons from the electrons transporting layer with the perovskite film [63]. A remarkable 20% stabilized power conversion efficiency was obtained through molecular doping in perovskite films [64]. Consequently, the conductivity of perovskite and electronic contract with the electrode material was improved, which facilitate the extraction of photoexcited holes from perovskite to the electrode substrate [64]. The schematic diagram of the hole transporting layer free perovskite solar cell structure is shown in Figure 12.

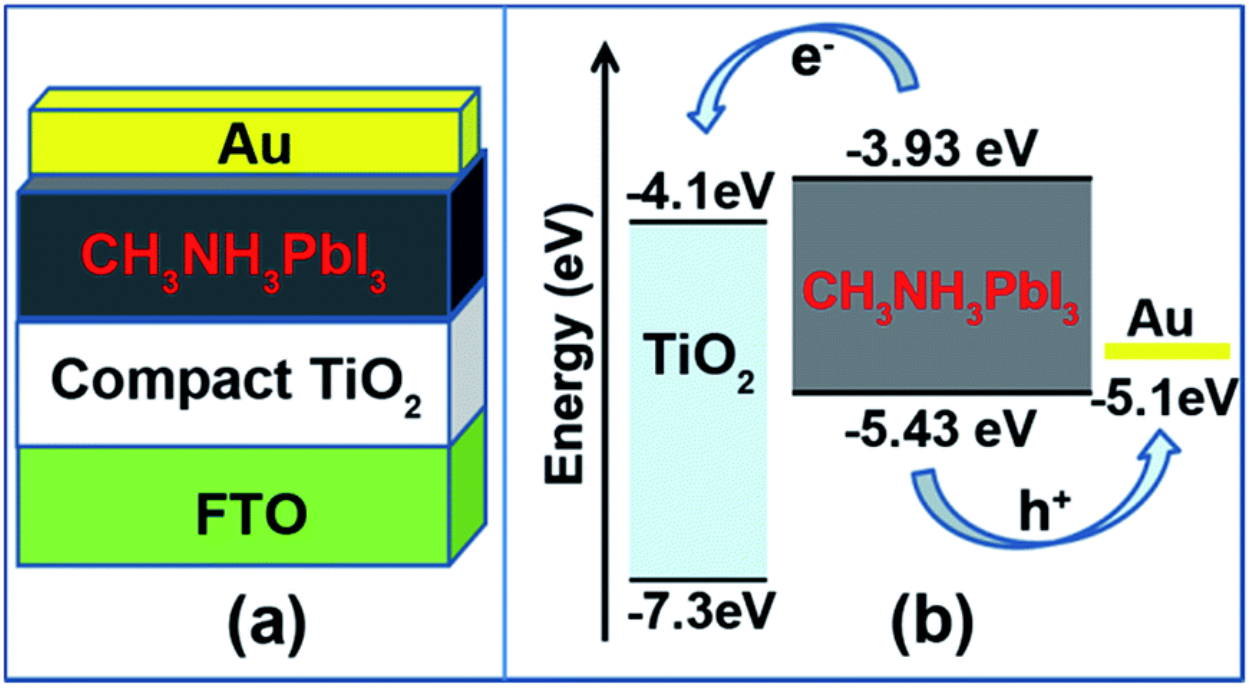

Figure 12. Schematic diagram of the (a) structure and (b) energy level alignment of the hole transporting layer free perovskite solar cell [65].

Materials for Perovskite Solar Cell

The choice of materials for each functional layers have significant effects on the device's electronic and optical properties and therefore on the overall performance of PSCs. In general, the materials used to fabricate the PSCs can be categorized into five different class: the transparent conductive oxide (TCO) layer, the electron transporting layer (ETL), the light harvesting perovskite material, the hole transporting layer (HTL), and the metal contact material.

At present, $CH_3NH_3PbI_3$ is the most common perovskite material that used in perovskite solar cell as light harvester. However, other perovskite materials like mixed cation, mixed halide, mixed cation mixed halide perovskites are also attaining increased attention as they are

advantageous over the traditional $CH_3NH_3PbI_3$ perovskite. Lead is known to be harmful to the environment. Therefore, scientists are researching to find effective alternative materials to lead to avoid the inherent toxicity. The reported bandgaps for $CH_3NH_3PbI_3$ are between 1.5 eV and 1.61 eV while the optimal bandgap for a single junction solar cell is between 1.1 eV and 1.4 eV [66]. There, the efficiency of PSCs can be further improved by lowering the bandgap of perovskite light absorbing materials. Although methylammonium lead iodide ($MAPbI_3$) offers excellent electrical and optical properties, researchers are trying to replace the methylammonium (MA) in $MAPbI_3$ / mixing different possible cations in place of MA due to the suboptimal band gap and long-term stability issues [67]. The modification in the monovalent cation can make a change in the Pb-I bond length and angle and therefore change in the overall band structure [33]. The exchange of MA ion with larger organic formamidinium (FA) ion results in a cubic structure of with slightly larger lattice, therefore a small decrease in the band gap [68]. In addition, Hanusch *et al.* found that $FAPbI_3$ is more stable thermally than both $MAPbI_3$ and $MAPbBr_3$ [69]. This finding strongly supports the idea that lager cation A in ABX_3 could further stabilize the perovskite structure.

Monovalent cation in perovskite can also be exchanged with inorganic materials such as Cs, Rb, as long as they maintain the range of tolerance factor. MA, FA and Cs based perovskite ($MAPbI_3$, $FAPbI_3$, and $CsPbI_3$) fall into the range of tolerance factor of 0.8 to 1.0 [35]. Li, Na, and K based perovskite fall outside of the established range of tolerance factor while $RbPbI_3$ fall outside by a small margin [35]. Therefore, although Rb has excellent oxidation stability, it cannot be used in perovskite alone. $CsPbI_3$ also exhibit excellent thermal stability, however, it does not possess an ideal band gap (1.73 eV) [70]. Due to the limitation of pure single cation halide perovskite, researchers focused to developed mixed cation mixed halide perovskite. In the

double cation perovskites, a small fraction of MA with FA in perovskite shows better crystallization result into photoactive black phase and therefore, better structural and thermal stability than that of pure MA or FA perovskite [22].

Besides organic MA-FA mixed cation perovskites, inorganic cations can be mixed with the organic monovalent cations. Choi *et al.* found that 10% Cs doping in $MAPbI_3$ improve the device efficiency up to 40% by improving the light absorption and morphology [71]. Lee et al. also found that Cs-doped perovskite showed improved photo and moisture stability than pristine $FAPbI_3$ [72]. Cs was also explored in more complex combination i.e. Cs-MA-FA. The triple cation based PSCs showed more reproducibility and thermal stability than MA-FA based PSCs [70]. Although Rb cannot be used in perovskite in alone, because of the inherent oxidation-stability they can be used in perovskite with other monovalent cations. Saliba *et al.* developed different cationic combination such as RbFA, RbCsFA, RbMAFA, and RbCsMAFA of perovskite which showed consistent device performance compared to previously explored triple cation based PSC device performances [35].

The optoelectronic properties of perovskite can be tuned by replacing or mixing halogen. From the photovoltaic perspective, each perovskite has its certain benefits. $MAPbI_3$ is suitable for single bandgap light absorber, whereas $MAPbbr_3$ and $MAPbCl_3$ are useful in tandem applications and light emitting devices respectively [68]. Moreover, mixed halide based perovskite can have additional benefits. Lee *et al.* found that mixed halide perovskite showed enhanced stability than $CH_3NH_3PbI_3$ perovskite during processing in the air [26]. Noh *et al.* also found that 20-29% Br into halide perovskite significantly improve the stability while maintaining the efficiency [73]. In addition, it is also possible to design mixed cation mixed halide perovskite by uniting their benefits and evading their drawbacks. Jeon et al. explored mix halide mixed

cation perovskite which has several benefits over the other combination of perovskites such as $MAPbI_3$, $FAPbI_3$, and $MAPb(I_{0.85}Br_{0.15})_3$ [22]. Although lead-based perovskite solar cells showed tremendous progress in the past few years, the toxicity of lead hinders the commercialization of PSCs. Recently, researchers are trying to find the less toxic / nontoxic functional materials to replace lead.

The choice of the electron transporting material is crucial for getting good performance. Organic and inorganic materials are used as the electron transporting materials based on the device architecture. Usually, organic materials are used in the inverted PSCs, and inorganic materials are used in regular PSCs. For an ideal electron transporting material, it should have an energy level that is compatible with perovskite materials, which is essential to promote the injection of photogenerated electrons and reduce energy losses [74]. In addition, the materials should also possess innately high electron mobility [74]. The energy level of commons organic and inorganic electron transporting materials that are used in PSCs are shown in Figure 13 and Figure 14 respectively. Some common inorganic electron transporting materials are TiO_2, SnO_2, ZnO, In_2O_3, WO_X, CeO_X [75–80]. Among them, titanium dioxide (TiO_2) is the most popular electron transporting material used in the regular n-i-p PSCs due to their excellent electron transporting properties [81]. Although ZnO have higher electron mobility than TiO_2 and can be generated though a low-temperature process, ZnO is known to be chemically unstable [82,83]. SnO_2 also shows wide bandgap, high transparency and high electron mobility [76,84].

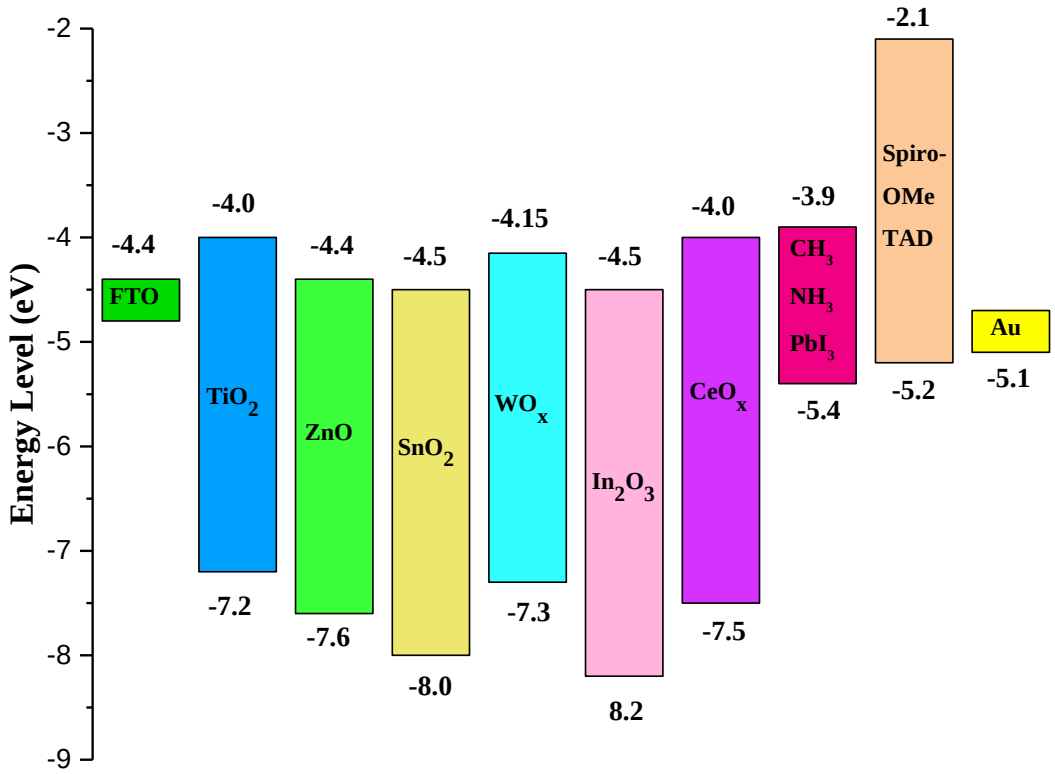

Figure 13: Energy levels of different inorganic materials acting as ETM with varying layers of PSCs.

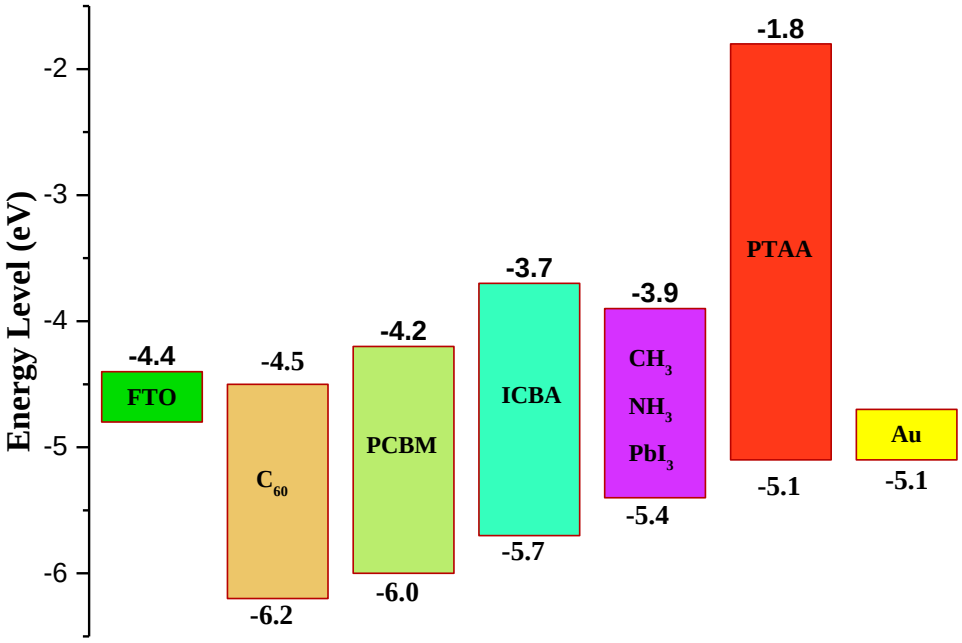

Figure 14: Energy levels of various organic materials working as ETM with different layers of PSCs.

The choice of hole transporting materials also has a significant effect on determining the overall performance of PSCs. The primary function of hole transporting materials is to act as hole-selective contact to extract the photo-generated holes and carry these holes to the counter electrode. It can also obstruct the direct contact between the perovskite and counter electrode [85]. Consequently, it prevents the charge recombination and enhances efficiency. For an ideal HTM, it should have a well-matched highest occupied molecular orbit (HOMO) energy level relative to the perovskite layer, good hole mobility, good thermal and photochemical stability [86]. Organic, inorganic, polymeric and carbon materials are used as hole transporting materials in PSCS. The energy level of commons hole transporting materials that are used in PSCs are

shown in Figure 15. Small molecules HTMs such as sprio-OMeTAD offer relatively simple processing and extensive modifiability [87]. However, it increase the fabrication cost due to the necessity of addition of ionic additives in it to increase the conductivity and hole mobility [88]. Polymeric materials such as polyaniline (PANI), poly(triarylamine) (PTAA) and poly(3-hexylthiophene-2,5-dipl) (P3HT) are potentially cheaper alternative than the small molecules and offer higher hole mobility [89–91]. However, the small molecules show promising result than the other polymeric HTMs, there spiro-OMeTAD is widely using the perovskite solar cells [92]. Inorganic materials such as NiO, CuSCN and CuI also explored as HTMs in perovskite solar cells due to their intrinsically high stability, high internal charge mobility and relatively low cost [86–88]. However, till now the use of inorganic materials is limited in perovskite solar cells due the slow progress towards the development of inorganic HTMs and the solvent that used to prepare the inorganic HTM solution partially dissolve or degrade the perovskite materials [88].

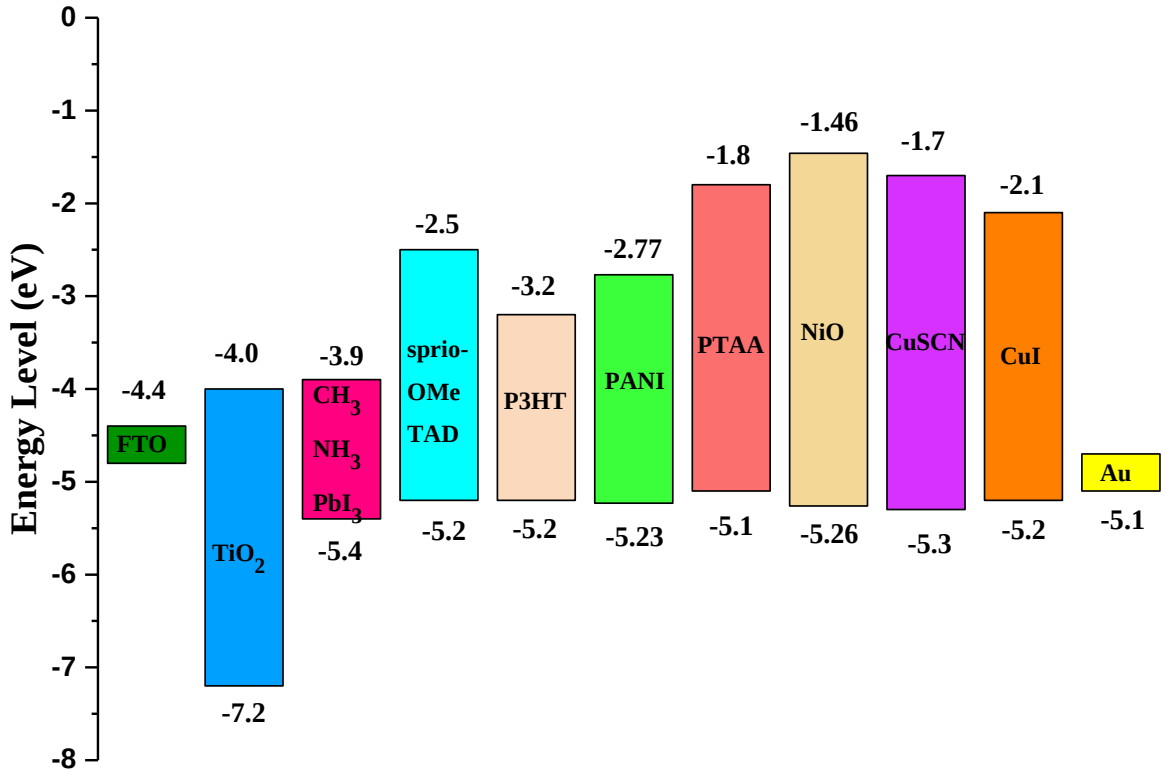

Figure 15: Energy levels of different materials acting as HTM with different layers of PSCs.

Fiber shaped Perovskite Solar Cells

Wearable / portable electronics have been becoming an essential part of our daily life with the ever-increasing importance of electronics in modern society. To fulfill the high demand for next-generation smart products for daily use, it is essential to develop flexible optoelectronic devices and then incorporate them into clothing, backpacks and other flexible objects [96]. Flexible fiber shaped energy generating devices will play a crucial role in the production and development of practical e-textiles. Conventional perovskite solar cell devices are mainly based

on a rigid substrate such as fluorine-doped tin oxide (FTO) or indium tin oxide (ITO) coated glass substrates. Their rigidity, weight, and frangibility limit the integration of the PSC devices into portable and wearable electronics [38]. To overcome this problem, conductive fiber / wire type substrate could be a potential alternative. These substrates will be suitable for contexture / importation into textiles materials.

Recently, a few numbers of research efforts have been conducted to construct flexible fiber / wire based perovskite solar cells. The very first fiber shaped PSCs was developed by Peng *et al.* [39]. They utilized transparent multiwall carbon nanotube (MWCNT) sheet and stainless steel (SS) fiber as the counter and working electrode respectively and obtained a maximum power conversion efficiency of 3.3% (Figure 16) [39]. However, the challenging part of their experiment was to obtain a continuous compact layer of TiO_2 and deposit the m-TiO_2 layer uniformly on the working electrode. Later, Lee et al. successfully developed a novel dimple compact layer of TiO_2 on the working electrode and used silver nanowire and Ti wire as the counter and working electrode respectively for the fiber-shaped PSC, and they were able to obtain a maximum PCE of 3.85% (Figure 17) [40]. The increased surface area of dimple compact layer of TiO_2 helps to improve the contact between the substrate and mesoscopic scaffold resulting in a reduction of the electrical resistance [40]. Although using transparent, conductive and flexible Ag NWs is counter electrode advantageous, the deposition process of Ag NW may have harmful effects on the perovskite layer. Hu *et al.* further integrated the traditional architecture for PSCs into fiber format by utilizing Ti wire and gold wire as working and counter electrode respectively and obtained a maximum PCE of 5.35% (Figure 18) [97]. They demonstrate that this fiber-based PSCs are highly symmetrical and can harvest solar energy from 3D space regardless of the direction of the incident light [97].

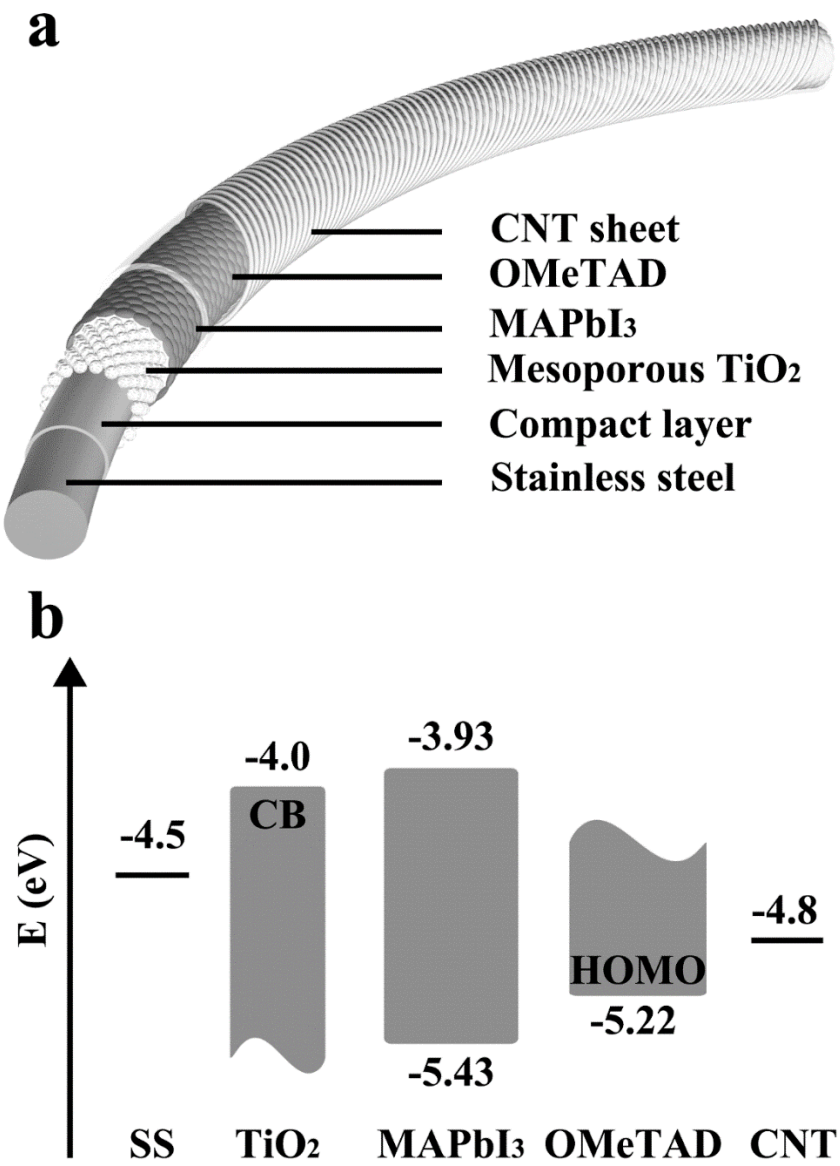

Figure 16: Schematic diagram of a fiber-shaped PSC: (a) structure - stainless steel (SS) as anode and carbon nanotube (CNT) as the cathode and b) energy-level diagram [39].

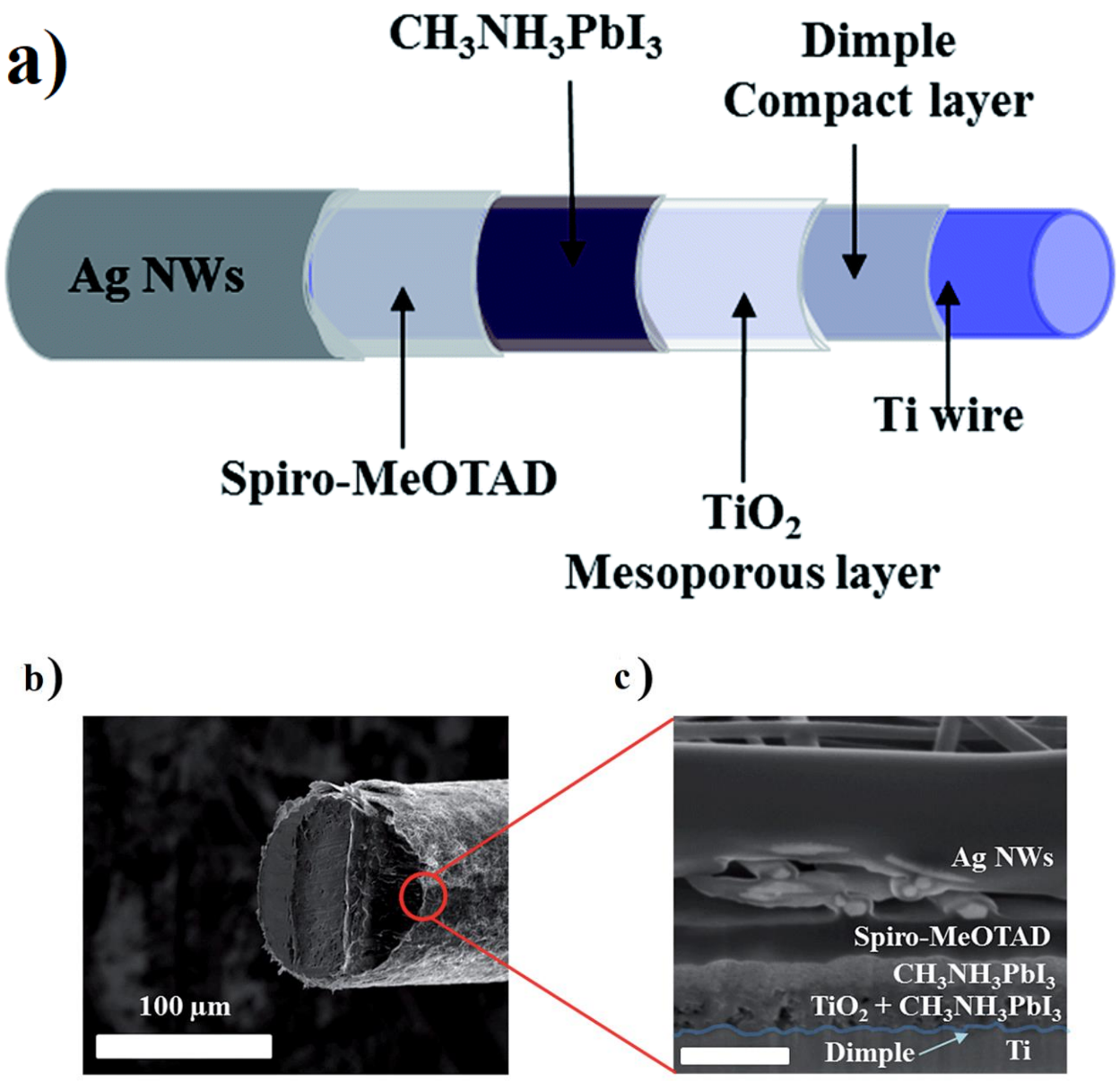

Figure 17: (a) Schematic illustration of the fiber-shaped PSC; silver nanowires (Ag NWs) as the counter electrode and Ti wire as the working electrode, (b) SEM image of the fiber-shaped PSC device (c) magnified image – scale 500nm [40].

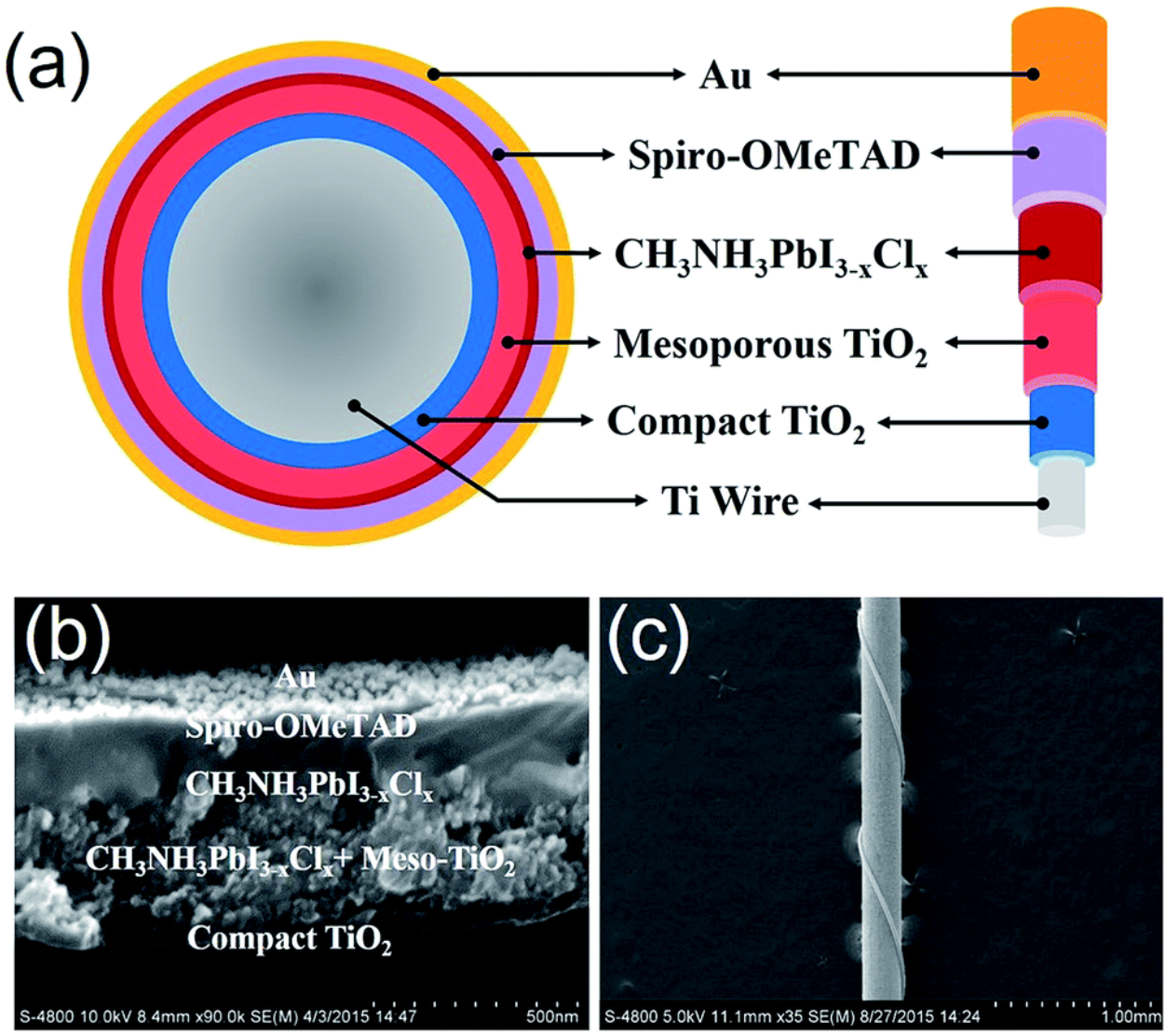

Figure 18: Schematic illustration of the fiber-shaped perovskite solar cell: (a) structure. (b) SEM cross-sectional image. (c) Image of typical FPSC [97].

With advancement in fiber-shaped solar cells, TiO_2 nanotubes have also garnered great interest due to their unique morphology. Wang et al. developed wire shaped PSCs based on TiO_2 / Ti wire for the first time through a successive dip coating process (Figure 19) [98]. Although they were able to obtain a maximum of 1.16% of PCE, the simple fabrication process allows being a potential candidate for large-scale cheap manufacturing. For being commercialized, it is

also necessary to withstand the stress produce during stretching and bending beside high efficiency and stability. Otherwise, the produced fiber shaped flexible cells will break / fracture and will lose the operational capability after a short period of time. Considering this issues, Deng *et al.* developed elastic perovskite solar cells utilizing CNT based conductive fiber and spring-like modified Ti wire as the counter and working electrode respectively (Figure 20) [99]. They obtained a power conversion efficiency ranging from 0.99% to 1.12%, and the cells maintained stable energy conversion efficiencies under stretching [99].

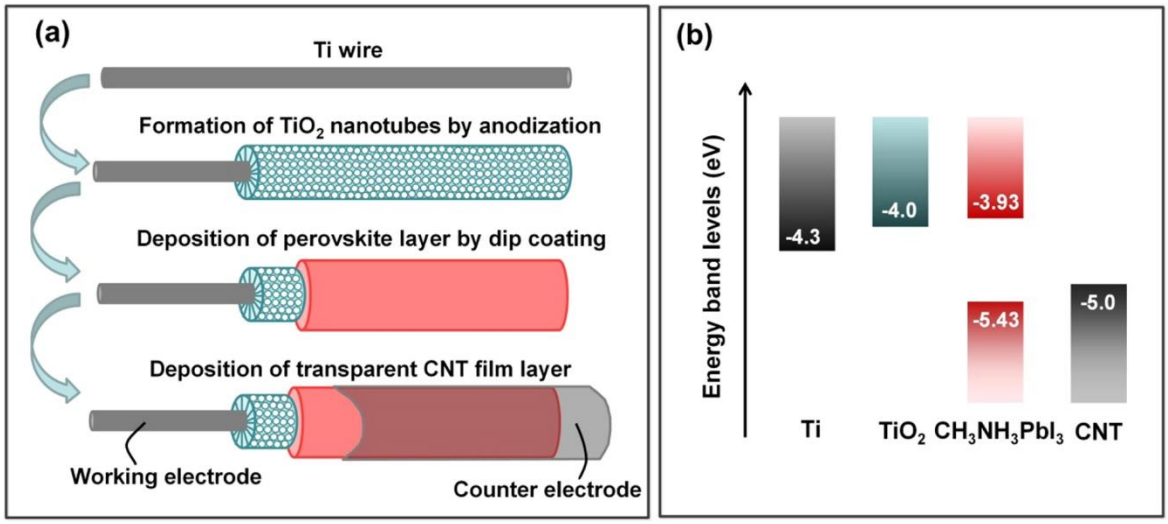

Figure 19: Schematic representation of a wire-shaped perovskite solar cell: (a) device architecture and fabrication process; (b) energy-level diagram [98].

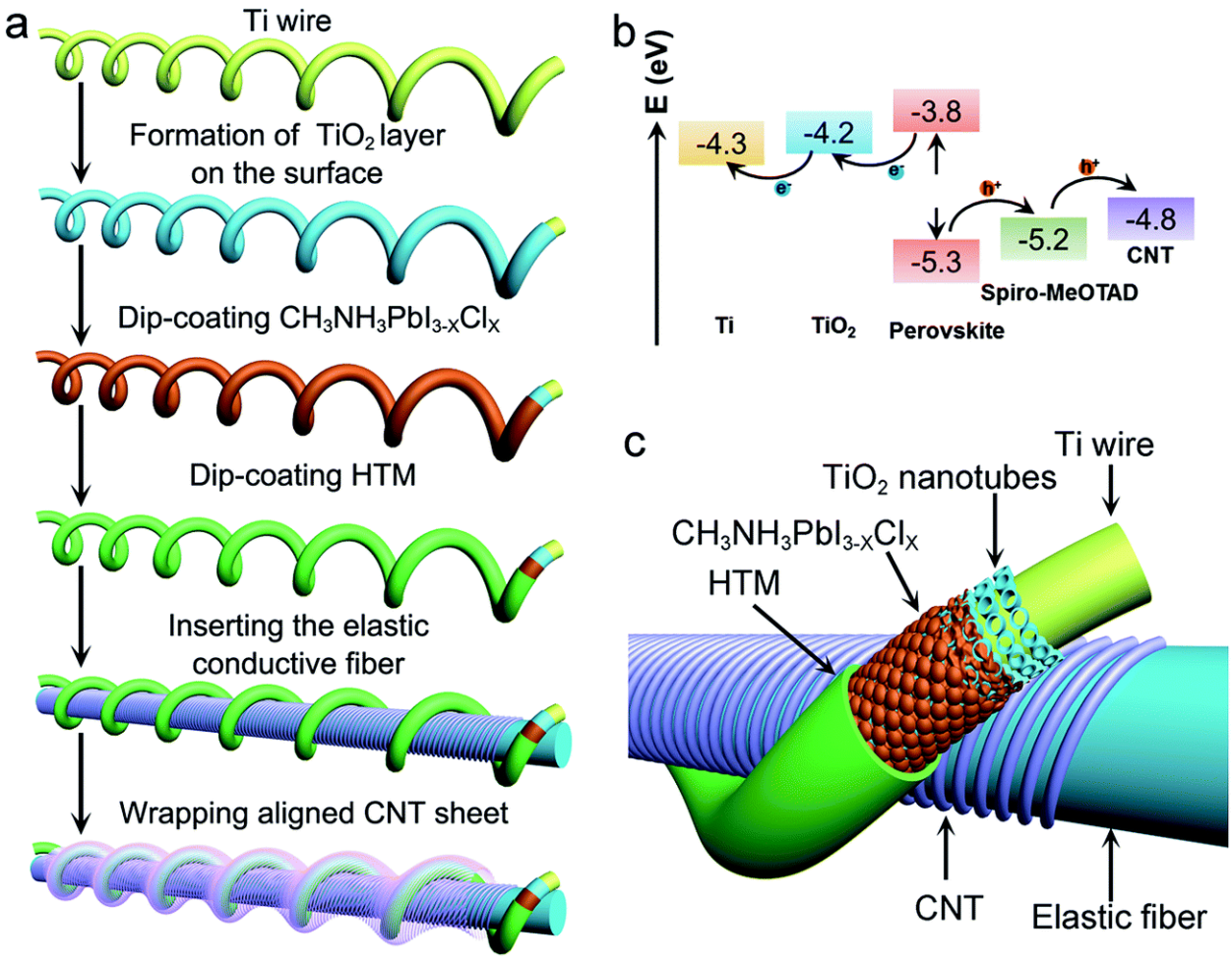

Figure 20: Schematic representation of the elastic PSC in fiber format. (a) Fabrication process (b) energy level diagram (c) device structure [99].

Carbon Nanotube Yarn

Carbon nanotube-based materials have gone through tremendous progress in the past few decades. Carbon nanotubes were first discovered by Iijima *et al.* in 1991 [100]. Due to their excellent physical and chemical properties, they have been using in a variety application in both industrial and research settings such as batteries, supercapacitors, solar cells, sensors, actuators, drug delivery systems, etc [5,101–106]. Carbon nanotubes are allotropes of carbon [107]. They

are seamless cylindrical shaped consisting of one or more layers of graphene with open or closed ends [108]. Depending on the number of walls present in the tube, it can be classified as single-walled carbon nanotubes (SWCNT), and multi-walled carbon nanotubes (MWCNT) [109].

Unlike platinum, gold or silver, carbon nanotubes have high electrochemical activity and interactive surface [5]. They also have excellent charge transport characteristics, chemical intentness as well as mechanical robustness [101]. The high aspect ratio (length to diameter ratio) and high surface area also favorable for exciton dissociation and charge carrier transport activity [110]. Due to their lightweight, excellent mechanical, electrical and chemical properties, they have the potentiality to replace the metal wire in solar cells [42,111]. When the CNTs are used in solar cells, they can efficiently extract photo-generated charges and improve the overall resiliency and stability of the cells. CNT sheets successfully used in perovskite solar cell as counter electrode material [99]. However, the carbon nanotube yarns exhibit better surface with entangled and inter-aligned CNTs than carbon nanotube sheet and films [42,112].

CHAPTER III

METHODOLOGY

Preparation of Working Electrode

The diameter of single carbon nanotube yarn used was 25 µm (Nancomp Technologies Incorporated, USA). The preparation of working electrode started with sintering to remove the polymer coating applied to the CNT yarns upon manufacturing. CNT yarns were sonicated in water and then rinsed with acetone, water, and 2-propanol. After rinsing with 2-propanol, the yarns were dried at room temperature and then functionalized by treating with 70% HNO_3 for 12 hours with continuous stirring at 50 rpm. After functionalizing, the CNT yarns were rewashed with acetone, water, and 2-propanol and dried at room temperature. Six CNT yarns were twisted together to form the working electrode.

Preparation of Electron Transporting Layer

The preparing of the electron transporting layer started with coating a nanoporous TiO_2 layer on the CNT yarn. 50 ml 2-propanol, 5.92 ml titanium isopropoxide, and 1.39 ml trimethylamine were mixed in a beaker under vigorous stirring for five mins to prepare solution A. Solution B was of 50 ml 2-propanol, 3 ml hydrochloric acid, and 0.72 ml water were stirred for five mins. Then, the two as-prepared solutions were mixed and stirred for another 30 mins.

The working electrodes were immersed into the as-prepared solution for 30 seconds followed by calcination at 70°C for five mins. The yarns were recalcined at 95°C for another five mins. Preparation of microporous solution started by mixing 15 ml of deionized (DI) water, 1 ml of glacial acetic acid, three drops of triethylamine and 5.921 ml of titanium under vigorous stirring for five mins. Another solution was prepared by mixing 15 ml DI water and 0.25ml 70% nitric acid. The as-prepared two solutions were then mixed and stirred for another five mins before hydrothermally treated in an autoclave at 240°C for 12 hours. 2.6 grams of polyethylene glycol was added to the solution followed by evaporation 50% of the solvent under vigorous stirring at 100°C. The microporous TiO_2 solution was dip-coated on the CNT yarn followed by calcination at 300°C for five mins. The coating and calcination process was repeated four times.

Preparation of Perovskite Layer

Methylammonium iodide (CH_3NH_3I) was synthesized using methylamine and hydroiodic acid according to a reported procedure [113]. First, methylamine (12 ml, 33 wt% in absolute ethanol, Aldrich) and hydroiodic acid (5ml, 57 wt% in water, Aldrich) were reacted in a 100 ml round-bottom flask at 0°C for two hours under continuous stirring. The precipitates were recovered by evaporating the solvent at 60°C for one hour using a rotary evaporator. The products were dissolved in ethanol, recrystallized by adding a certain amount of diethyl ether. Finally, the product was dried at 60°C for 24 hours in a vacuum oven.

The inorganic-organic halide perovskite precursor solution was prepared by mixing 461 mg of PbI_2, 159 mg of CH_3NH_3I, 78 mg of dimethyl sulfoxide (DMSO) (molar ratio 1:1:1) in 600 mg dimethylformamide (DMF) solution for one hour at room temperature under continuous

stirring [114]. The as-prepared TiO2 coated working electrode was dip coated into the perovskite precursor solution for 30 sec and then annealed for five mins at 100°C in nitrogen followed by cooling down to room temperature. The process was repeated, and finally, annealing was carried out at 100°C for 60 mins in nitrogen.

Preparation of Hole Transporting Layer

The hole transporting material (spiro-OMeTAD (2,2,7,-7-tetrakis(N,N-di-p-methoxyphenylamine)-9,9′-spirobifluorene)) solution was prepared by dissolving 72.3 mg of spiro-OMeTAD in 1 ml chlorobenzene, and then 17.5 µL of lithium bis(trifluoromethanesulfonyl)imide (Li-TFSI) solution (520 mg Li-TSFI in 1 ml acetonitrile, Sigma Aldrich, 99.8%) and 28.8 µL of 4-tert-butyl pyridine (TBP) were added to this solution [115]. The as-prepared twisted yarn was dip coated in spiro-OMeTAD solution for two mins followed by annealing in nitrogen at 100°C.

Preparation of Counter Electrode

Single CNT yarn was used as the counter electrode (CE) The carbon nanotube yarns were treated according to the procedure mentioned above. Then CEs were platinized using Compact Plasma Sputtering Coater for 60 s at 1.5KV and 5mA. Then, the CE was wrapping on the outer surface of the WE to produce the three-dimensional CNT yarn based PSC.

Device Characterization

The morphology of the electrode materials was investigated using Zeiss Sigma VP scanning electron microscope (SEM). We used a Bioscope Catalyst atomic force microscope (Bruker) for AFM measurements. The ScanAsyst mode was used to image the samples in air. This mode is a PeakForce Tapping based image optimization technique that enables the highest resolution. A triangular silicon nitride cantilevers (Bruker, scanasyst-air, spring constant 0.4 N/m) were used for all measurements. AFM images were recorded in the air at room temperature each step of the functionalization process. FTIR spectra were characterized by a Bruker Tensor 27 FTIR spectrometer in the range of 4000-400 cm^{-1}. The device photocurrent-voltage performance was characterized using VersaSTAT3 (Electrochemical system with EIS capability, Princeton Applied Research, USA) running cyclic voltammetry with a potential scan rate of 50 mVs^{-1}. A Honle solar simulator 400 (light intensity 100 $mWcm^{-2}$) was used to simulate the sunlight for illuminating the cell with an AM 1.5G spectrum.

CHAPTER IV

RESULT AND DISCUSSION

The schematic fabrication process of the as-prepared CNT yarn based perovskite solar cell is shown in Figure 19. The CNT yarns that were used to construct the cells consisted of a large number of multiwalled carbon nanotubes. The yarn was treated with acid to remove the polymer which was applied during the manufacturing. The acid treatment improved the surface smoothness of the yarns significantly. As shown in Figure 19, the electron transport layer (TiO_2) was obtained through two steps for faster electron transportation. In the first step, the nanoporous TiO_2 layer was coated on the six twisted CNT yarns. In the second step, a microporous TiO2 was formed on the nanoporous TiO_2 coated CNT yarn. The nanoporous TiO_2 layer is the foundational layer of the microporous layer and exposes a surface for better attachment of the major microporous coating [42]. The calcination of the TiO_2 with $TiCl_4$ enhance the surface area and confirms that the irregularities are covered with the TiO_2 layer [116]. A spin coating process is typically better for attaining uniform functional layers. However, this process is not ideal for yarn / fiber shaped devices due to difficulties in penetrating the yarn shape. Therefore, all the coating process are done through a simple coating process. The perovskite layer was deposited over the TiO_2 coated CNT yarn through a simple single dip-coating process followed by a hole transporting layer (spiro-OMeTAD) to facilitate the transportation of holes to the counter electrodes. Ionic additives such as lithium bis(trifluoromethanesulfonyl)imide (Li-TFSI) and 4-tert-butyl pyridine (TBP) are in the hole transporting materials solution to enhance the

innate the conductivity and hole mobility of the spiro-OMeTAD. Finally, the cells were wrapped with a platinized single CNT yarn, which works as the counter electrode. The platinization on CNT yarn increases the conductivity without altering the physical properties of the yarn [43]. The flexibility of the carbon nanotubes yarns allows as wrapping process at any pitch rate as shown in Figure 21. Also, it ensures the proper contact between the working and counter electrode.

The structure of the complete three-dimensional perovskite solar cell is shown in Figure 22. The CNT yarn based PSC works based on the same mechanism of the traditional PSC and other fiber-based PSC devices. When sunlight hits the devices, light (incident photons) is absorbed by the perovskite ($CH_3NH_3PbI_3$), and then free charge carriers are produced from the incident photons. Upon generating the free charges, electrons and holes are separated to generate an electric field followed by transfer to the electrons transporting layer (TiO_2) and hole transporting layer (Spiro-OMeTAD) respectively. Finally, these electrons and holes are collected by the working electrode (6 twisted CNT yarn) and counter electrode (platinized CNT yarn).

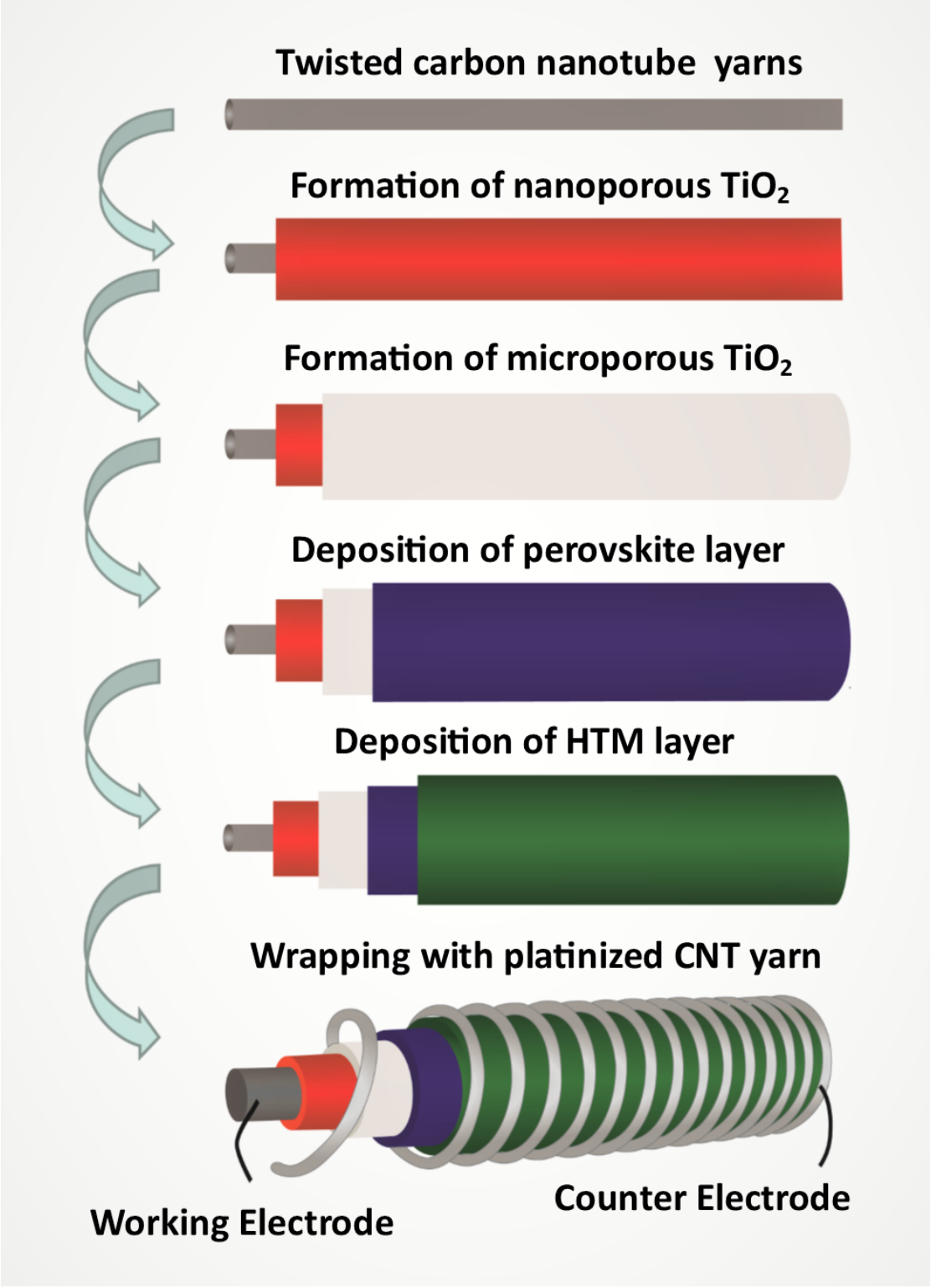

Figure 21: Schematic fabrication process of the three-dimensional CNT yarn based perovskite solar cell.

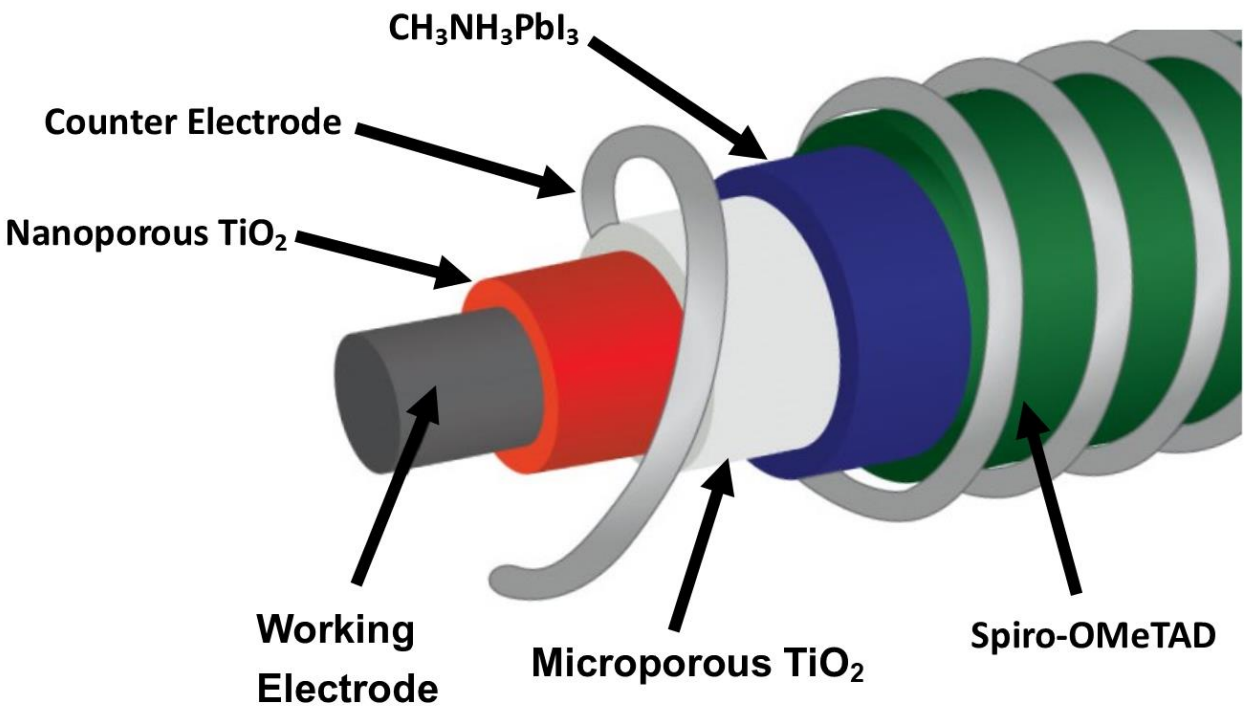

Figure 22: Structural representation of the three-dimensional CNT yarn based perovskite solar cell.

The morphology of CNT yarns and different functional layers of perovskite solar cells were characterized by scanning electron microscopy (SEM) and atomic force microscopy (AFM). Figure 23a and Figure 23b shows the SEM image of CNT yarn that used to construct the cell. CNT yarns consisted of a larger number of multiwalled carbon nanotubes. The CNT yarns are highly interalinged which is vital for fast electron transport and provides them with excellent electrical conductivity and vertical alignment [43]. As shown in Figure 23c, high coverage of the perovskite materials on the TiO_2 coated CNT yarns surface was attributed, which is a key to obtaining high photovoltaic performance. In addition, a uniform hole transporting layer was achieved through a simple dip coating process on the perovskite firm (Figure 23d). High resolution AFM imaging were recorded on the uncoated CNT yarn and each step of the coating

process of perovskite solar cell, which was displayed in Figure 24. As shown in Figure 24a, AFM image of the uncoated CNT yarn reveals the individual carbon nanotubes. The highly interaligned structure is advantageous because it increases the electron transportability of the CNT yarn electrode [116]. Figure 24b shows the AFM imaging of the CNT yarn when it is fully covered with the nanoporous and microporous TiO_2 coating. The TiO_2 layer is uniformly deposited and well defined on the counter electrode surface. In addition, single (black arrow) and clusters (white arrow) of TiO_2 nanoparticles are present in the coating on the CNT yarn. Moreover, the high surface areas of the TiO_2 is beneficial for absorbing photoactive materials and therefore, improving the performance of the cell. Figure 24c shows the AFM image of the perovskite layer on the TiO_2 coated CNT yarn, which reveals a homogenous coating with two phases, one porous (black arrow) and the slightly rough (white arrow). The homogenous coating of the perovskite layer favors the deposition of the hole transporting layer and aids to decrease the interfacial resistance, resulting in the increase of the charge transportability at the interface [117]. Figure 24d shows a homogeneous porous structure of the hole transporting layer (spiro-OMeTAD).

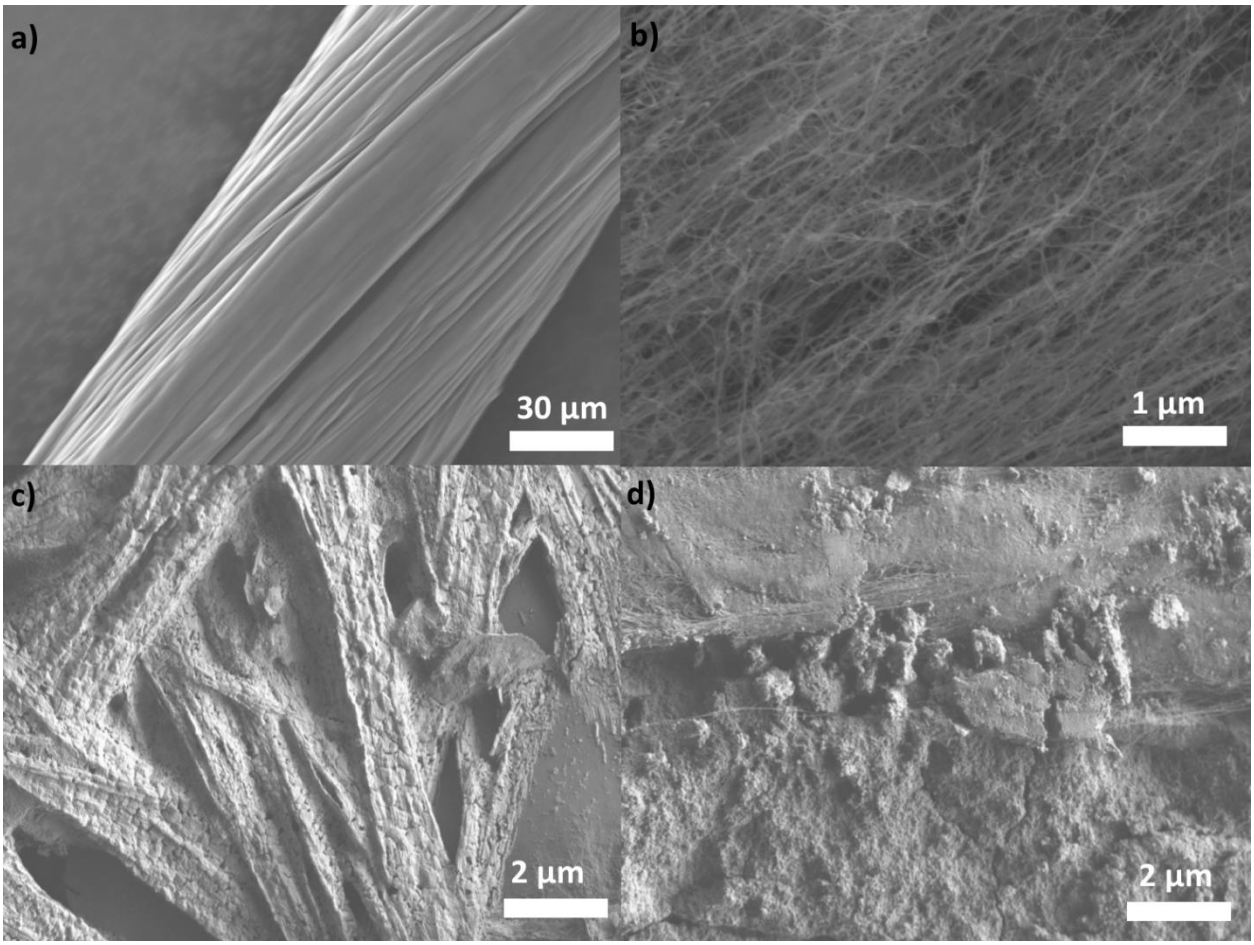

Figure 23: SEM images of different functional layers of perovskite solar cell (a) CNT yarn used to construct the cells (b) high-resolution SEM image (zoomed on the image a) (c) perovskite layer on TiO2 coated CNT yarn (d) hole transporting layer on perovskite.

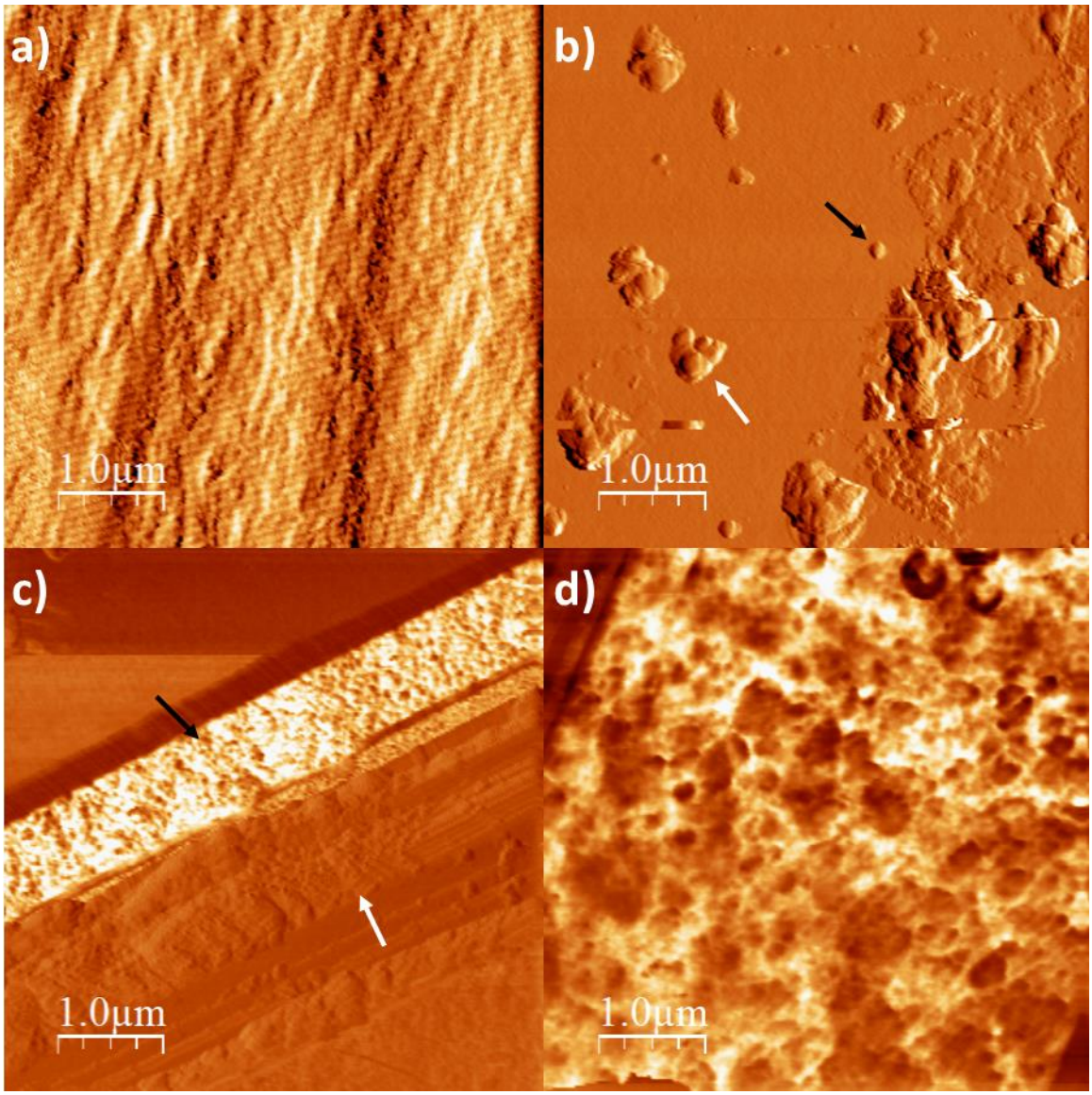

Figure 24: AFM image of different functional layers of perovskite solar cell (a) CNT yarn before coating (b) CNT yarn after coating with TiO_2 and annealing with $TiCl_4$ (c) perovskite layer on TiO_2 coated CNT yarn (d) spiro-OMeTAD coating TiO_2 and perovskite layer.

Figure 25 reveals the FTIR spectral features of the TiO_2, perovskite ($CH_3NH_3PbI_3$) and Methyl ammonium iodide (MAI or CH_3NH_3I) in the wavenumber range of 400-4000cm^{-1}. The FTIR spectrum of TiO_2 shows that the band around 3400 cm^{-1} refers to the characteristics of associated hydroxyl groups. The band observed at 3100 cm^{-1} corresponds to the stretching

vibration of the hydroxyl group O-H. The hump observed around 1600 cm^{-1} corresponds to the bending modes of water Ti-OH and the peak around 1250 cm^{-1} is related to Ti-O modes. On analysis of the spectrum of perovskite we have: the absorption features in the range of 1400 – 1500 cm^{-1} corresponds to the symmetric NH_3^+ bending and asymmetric CH_3 bending while CH_3-NH_3^+ rocking and C-N stretching modes are present in the range of 800-1250 cm^{-1}. On the other hand, FTIR spectrum of methyl ammonium iodide (MAI or CH_3NH_3I) reveals that the band around 3400cm^{-1} can be attributed to N-H stretching and the bands observed around 1200cm^{-1} and 800cm^{-1} corresponds to the C-N stretching and NH_3 stretching respectively.

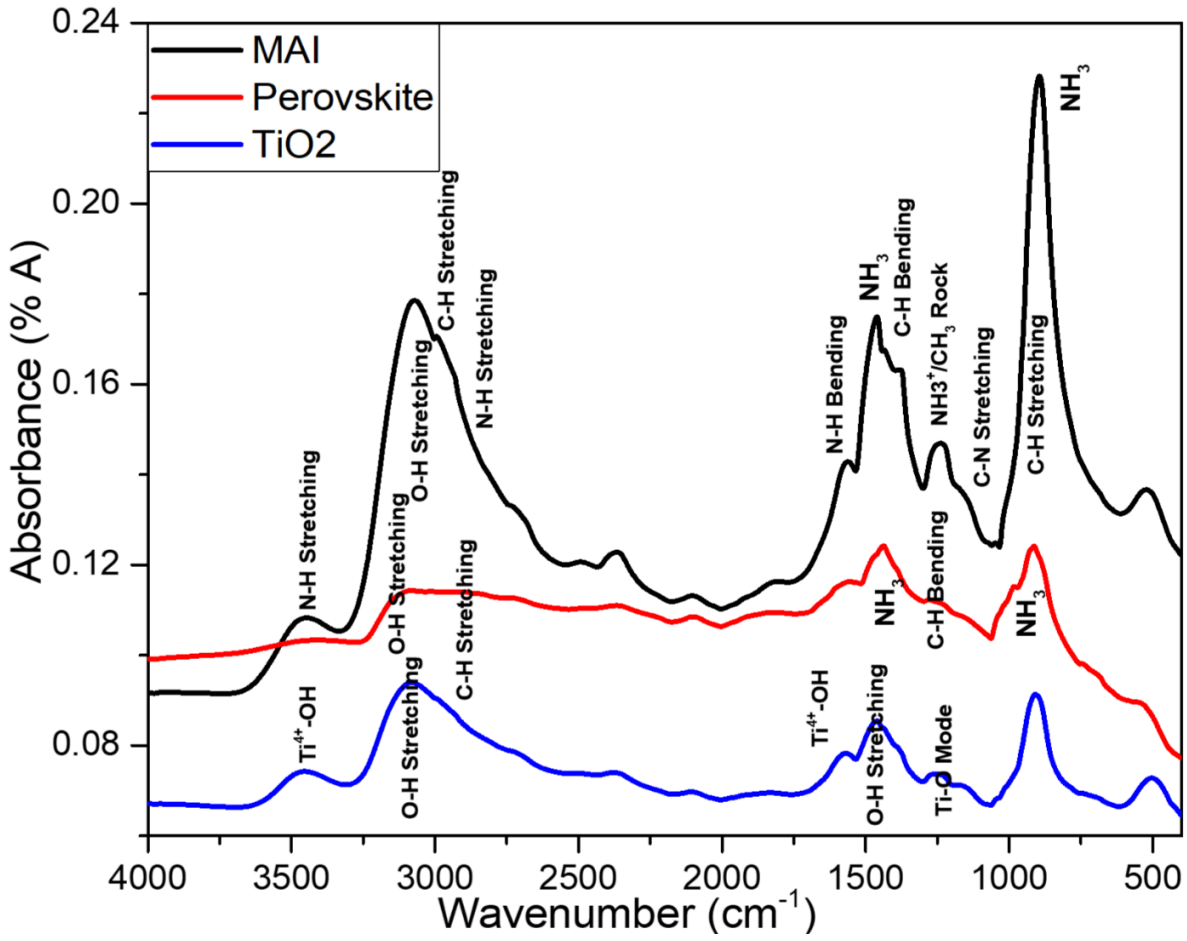

Figure 25: FTIR spectra of methylammonium iodide (MAI or CH_3NH_3I), perovskite ($CH_3NH_3PbI_3$) and TiO_2.

The photovoltaic cell characterization was carried out under AM 1.5 illumination using versastat3 under full sun. Figure 26a represents the current density – potential (J-V) characteristics curve of the cell-1 at 2.5 cm, 4.0 cm and 5.0cm cell length. It can be seen that current density highest when the cell is 5.0 cm in length whereas the cell potential is highest when the cell is 2.5 cm in length. With the decrease of the cell in length (5 cm to 2.5 cm), the current density falls from ~3.9 to ~1.8 mA/cm^2 while the potential rises from ~0.41 to ~0.80 V. This indicates that current density decreases with decreasing the cell in length and the potential increases with decreasing the cell in length. Figure 26b shows the current density – potential (J-V) characteristics curve of three different cells at same cell length (2.5 cm). The similar J-V performance proves the consistency of the cell performance of the prepared CNT yarn based PSCs. The three cells at 2.5 cm cell length produce high open current voltage and low short circuit current. This high V_{OC} results from the low recombination rate and the low Jsc could result from the incomplete coverage of the perovskite layer on the working electrode and not having the optimal thickness of the perovskite layer. Further optimization on the thickness of the perovskite and other functional layers will help to improve the photocurrent density and therefore improve the overall cell efficiency. However, it is difficult to point out a single factor for reduced cell performance as the cells consist of a number of components. Moreover, difficulties during the connection of the cells to the testing equipment (VersaSTAT3) can partially account for the reduced cell performance [116].

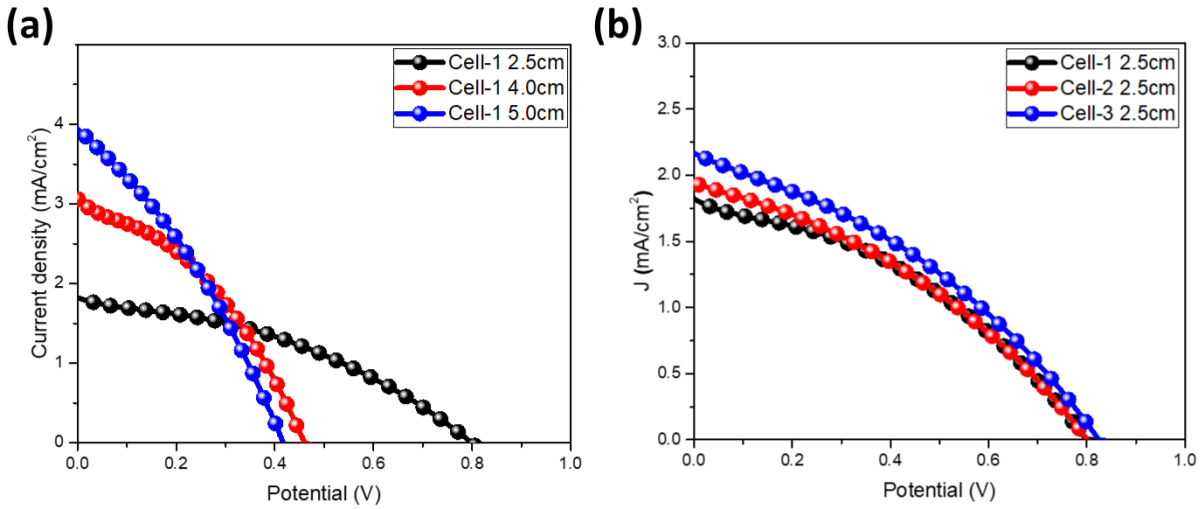

Figure 26: Current density vs potential (J-V) curve (a) cell 1 at different cell length (2.5cm, 4.0cm and 5.0cm) (b) cell 1, 2, 3 at 2.5 cm cell length.

The photovoltaic performance parameters such as current density J_{SC}, open current voltage V_{OC} of different cells at different cell lengths were investigated and summarized in Figure 27. The average value of Jsc increases with increasing the cell in length, and the maximum Jsc is recorded when the cell length in 4.5 cm. On the other hand, the average value of Voc decreases with increasing the cell in length, and the maximum Voc is recorded when the cell length is 2.5 cm. At 2.5 cm cell length, the cell also exhibited the highest power conversion efficiency. Other two photovoltaic performance parameter such as fill factor and power conversion efficiency of different cells at different cell lengths was calculated from the recorded current and potential data and summarized in Figure 28. The average fill factor of six efficient cells at each cell length is shown in Figure 28a. The average fill factor values slightly varies over the cell length from 2.0 cm to 5.0 cm. The values of fill factor of CNT based perovskite solar cells limited to 0.3-0.4, which is similar to that of Ti wire based PSCs [98]. Figure 28b shows the average PCE of different cells at different cell length. As reflected in Figure 28b, the power

conversion efficiency decreases with increasing cell in length, and maximum average PCE is recorded at 2.5 cm cell length. It can also be estimated the PSCs exhibit an average efficiency of 0.40% over cell length 2.0 cm to 5.0 cm.

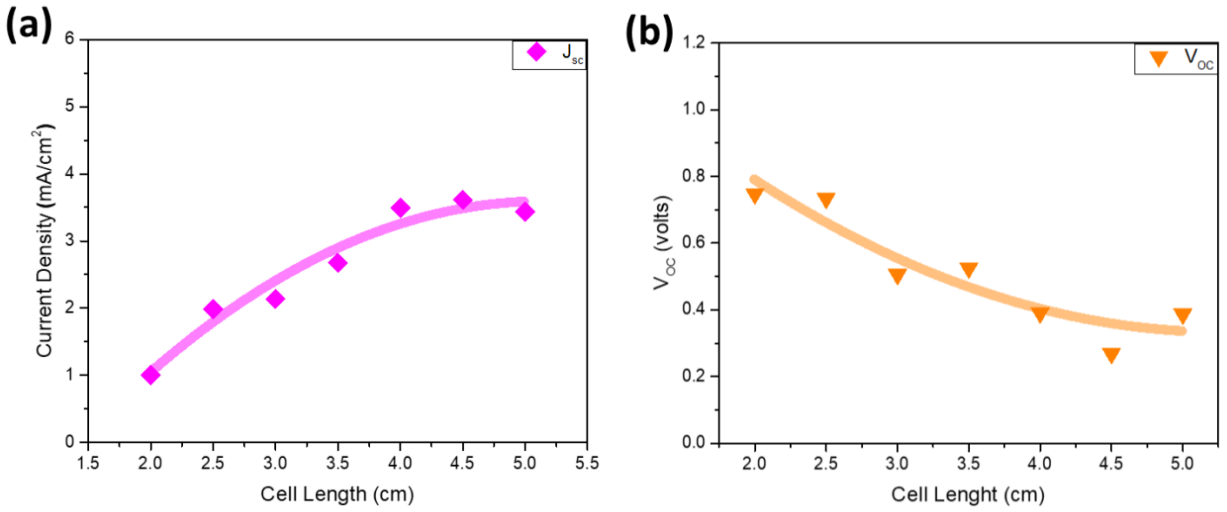

Figure 27: Average value of (a) current density (Jsc) (b) open current voltage (Voc) of different cells with respect to different cell lengths.

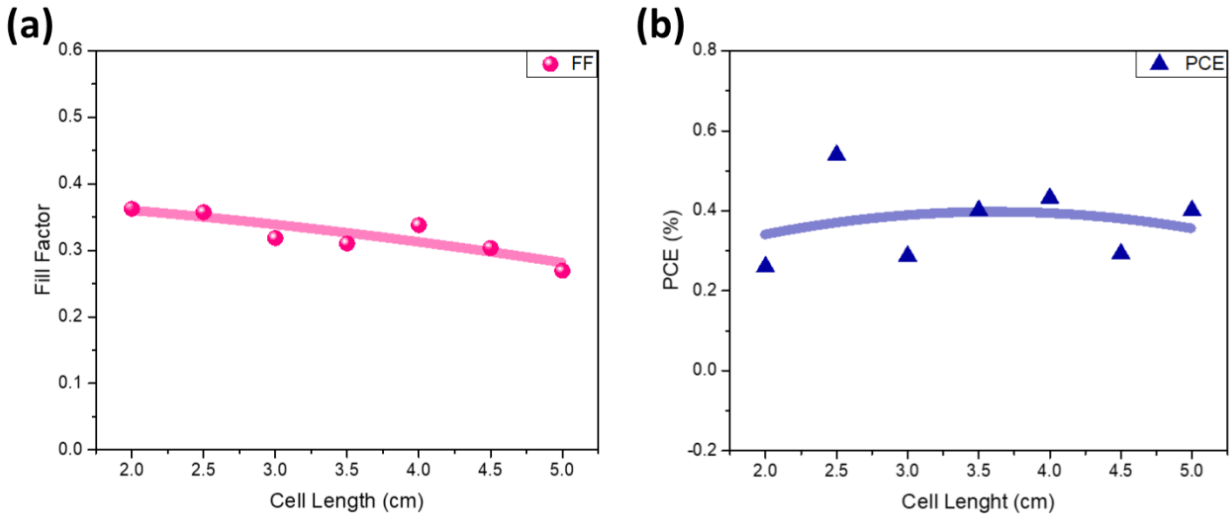

Figure 28: Average value of (a) fill factor (b) power conversion efficiency of different cells with respect to different cell lengths.

Figure 29a-b showed the design of a three dimensional (3D) sensing environment, which is constructed by placing a mirror beneath the cell to capture the incident light from both sides when sunlight hits the cell directly and the mirror. The sectional and vertical view of the cell is displayed in Figure 29a, and the optical image of a CNT yarn based perovskite solar cell is shown in Figure 29b. The simplicity and operational flexibility of the cell are increased the entwinement of the CNT yarns. In addition, the CNT yarn based working electrode has higher conductivity than that of semiconducting oxide, and it is also capable transferring the more photogenerated electrons to an external circuit than other conventional flat electrodes [41]. The photovoltaic performance of the most efficient cell among the prepared cells is shown in Figure 29c. This cell exhibits a maximum power conversion efficiency of 0.631% with a very high V_{OC} of 0.825 V, J_{SC} of 2.615 mA/cm^2 and FF of 0.353.

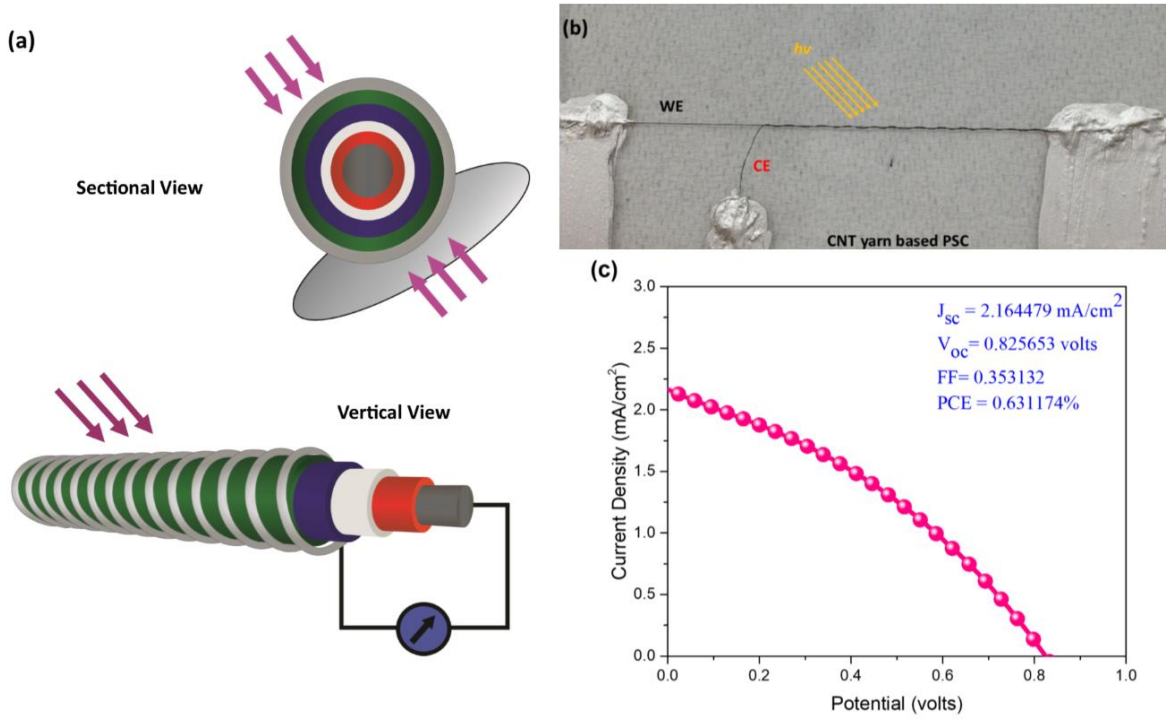

Figure 29: (a) Sectional and vertical view of perovskite solar cell (b) optical image of the CNT yarn based PSC (c) J-V curve of the most efficient CNT yarn based PSC.

CHAPTER V

CONCLUSIONS

Flexible solar cells based on carbon nanotube yarn have a great potentiality to integrate into e-textiles for next-generation power supply. An innovative, flexible fiber shaped perovskite solar cells has been developed by deploying carbon nanotube yarn as both the counter and the working electrode. The cells exhibited a high open current voltage of 0.825 V with a maximum power conversion efficiency of 0.631%. To the best of our knowledge, this is the first demonstration of the carbon nanotube yarns working as both the counter and the working electrode in perovskite solar cells. The flexibility and three-dimensional structural features of PSCs allow them to absorb incident photons from any direction and make them a potential candidate to incorporate into the next generation wearable and portable electronics. The excellent electrocatalytic interface with CNT yarn exhibited high surface exposure. The faster electrons transport and interaligned conductive CNT yarns with high surface area have a significant role in designing longer and more complex solar cells. The three-dimensional, all solid-state carbon nanotube yarn based perovskite solar cells open the opportunities to develop fiber shaped solar cells. Therefore, their ongoing investigation will be a promising strategy for the development of the next-generation photovoltaic devices.

REFERENCES

[1] Energy Production and Consumption in the United States | EBF 301: Global Finance for the Earth, Energy, and Materials Industries, (n.d.). https://www.e-education.psu.edu/ebf301/node/457 (accessed October 6, 2018).

[2] Biomass and waste fuels made up 2% of total U.S. electricity generation in 2016 - Today in Energy - U.S. Energy Information Administration (EIA), (n.d.). https://www.eia.gov/todayinenergy/detail.php?id=33872 (accessed October 6, 2018).

[3] F. Tasnim, S.A. Iqbal, A.R. Chowdhury, Biogas production from anaerobic co-digestion of cow manure with kitchen waste and Water Hyacinth, Renew. Energy. 109 (2017) 434–439. doi:10.1016/j.renene.2017.03.044.

[4] W.A. Hermann, Quantifying global exergy resources, Energy. 31 (2006) 1685–1702.

[5] J. Jaksik, H.J. Moore, T. Trad, O.I. Okoli, M.J. Uddin, Nanostructured functional materials for advanced three-dimensional (3D) solar cells, Sol. Energy Mater. Sol. Cells. 167 (2017) 121–132. doi:10.1016/j.solmat.2017.03.033.

[6] N.S. Lewis, D.G. Nocera, Powering the planet: Chemical challenges in solar energy utilization, Proc. Natl. Acad. Sci. 103 (2006) 15729–15735. doi:10.1073/pnas.0603395103.

[7] M.A. Green, Third generation photovoltaics: Ultra-high conversion efficiency at low cost, Prog. Photovolt. Res. Appl. 9 (n.d.) 123–135. doi:10.1002/pip.360.

[8] K.D.G.I. Jayawardena, L.J. Rozanski, C.A. Mills, M.J. Beliatis, N.A. Nismy, S.R.P. Silva, 'Inorganics-in-Organics': recent developments and outlook for 4G polymer solar cells, Nanoscale. 5 (2013) 8411–8427. doi:10.1039/C3NR02733C.

[9] G. Conibeer, Third-generation photovoltaics, Mater. Today. 10 (2007) 42–50. doi:10.1016/S1369-7021(07)70278-X.

[10] Home - Energy Explained, Your Guide To Understanding Energy - Energy Information Administration, (n.d.). https://www.eia.gov/energyexplained/ (accessed October 18, 2018).

[11] What is U.S. electricity generation by energy source? - FAQ - U.S. Energy Information Administration (EIA), (n.d.).

https://www.eia.gov/tools/faqs/faq.php?id=427&t=3,%20accessed:%20July,%202017. (accessed October 6, 2018).

[12] A. Kojima, K. Teshima, Y. Shirai, T. Miyasaka, Organometal Halide Perovskites as Visible-Light Sensitizers for Photovoltaic Cells, J. Am. Chem. Soc. 131 (2009) 6050–6051. doi:10.1021/ja809598r.

[13] H.-S. Kim, C.-R. Lee, J.-H. Im, K.-B. Lee, T. Moehl, A. Marchioro, S.-J. Moon, R. Humphry-Baker, J.-H. Yum, J.E. Moser, M. Grätzel, N.-G. Park, Lead Iodide Perovskite Sensitized All-Solid-State Submicron Thin Film Mesoscopic Solar Cell with Efficiency Exceeding 9%, Sci. Rep. 2 (2012). doi:10.1038/srep00591.

[14] W.S. Yang, J.H. Noh, N.J. Jeon, Y.C. Kim, S. Ryu, J. Seo, S.I. Seok, High-performance photovoltaic perovskite layers fabricated through intramolecular exchange, Science. 348 (2015) 1234–1237. doi:10.1126/science.aaa9272.

[15] G.E. Eperon, S.D. Stranks, C. Menelaou, M.B. Johnston, L.M. Herz, H.J. Snaith, Formamidinium lead trihalide: a broadly tunable perovskite for efficient planar heterojunction solar cells, Energy Environ. Sci. 7 (2014) 982–988. doi:10.1039/C3EE43822H.

[16] G. Xing, N. Mathews, S. Sun, S.S. Lim, Y.M. Lam, M. Grätzel, S. Mhaisalkar, T.C. Sum, Long-range balanced electron- and hole-transport lengths in organic-inorganic CH3NH3PbI3, Science. 342 (2013) 344–347. doi:10.1126/science.1243167.

[17] J.T.-W. Wang, J.M. Ball, E.M. Barea, A. Abate, J.A. Alexander-Webber, J. Huang, M. Saliba, I. Mora-Sero, J. Bisquert, H.J. Snaith, R.J. Nicholas, Low-temperature processed electron collection layers of graphene/TiO2 nanocomposites in thin film perovskite solar cells, Nano Lett. 14 (2014) 724–730. doi:10.1021/nl403997a.

[18] R.K. Misra, S. Aharon, M. Layani, S. Magdassi, L. Etgar, A mesoporous–planar hybrid architecture of methylammonium lead iodide perovskite based solar cells, J. Mater. Chem. A. 4 (2016) 14423–14429. doi:10.1039/C6TA06960F.

[19] Y. Shi, Y. Xing, Y. Li, Q. Dong, K. Wang, Y. Du, X. Bai, S. Wang, Z. Chen, T. Ma, CH3NH3PbI3 and CH3NH3PbI3–xClx in Planar or Mesoporous Perovskite Solar Cells: Comprehensive Insight into the Dependence of Performance on Architecture, J. Phys. Chem. C. 119 (2015) 15868–15873. doi:10.1021/acs.jpcc.5b02784.

[20] X. Ma, P. Tang, D. Liu, J. Zhang, L. Feng, L. Wu, Interface Engineering of Perovskite Solar Cells with Air Plasma Treatment for Improved Performance, ChemPhysChem. 18 (2017) 2939–2946. doi:10.1002/cphc.201700536.

[21] M. Hou, H. Zhang, Z. Wang, Y. Xia, Y. Chen, W. Huang, Enhancing Efficiency and Stability of Perovskite Solar Cells via a Self-Assembled Dopamine Interfacial Layer,

ACS Appl. Mater. Interfaces. 10 (2018) 30607–30613. doi:10.1021/acsami.8b10332.

[22] N.J. Jeon, J.H. Noh, W.S. Yang, Y.C. Kim, S. Ryu, J. Seo, S.I. Seok, Compositional engineering of perovskite materials for high-performance solar cells, Nature. 517 (2015) 476–480. doi:10.1038/nature14133.

[23] G.E. Eperon, V.M. Burlakov, P. Docampo, A. Goriely, H.J. Snaith, Morphological Control for High Performance, Solution-Processed Planar Heterojunction Perovskite Solar Cells, Adv. Funct. Mater. 24 (2014) 151–157. doi:10.1002/adfm.201302090.

[24] H. Tsai, W. Nie, P. Cheruku, N.H. Mack, P. Xu, G. Gupta, A.D. Mohite, H.-L. Wang, Optimizing Composition and Morphology for Large-Grain Perovskite Solar Cells via Chemical Control, Chem. Mater. 27 (2015) 5570–5576. doi:10.1021/acs.chemmater.5b02378.

[25] J.-H. Im, C.-R. Lee, J.-W. Lee, S.-W. Park, N.-G. Park, 6.5% efficient perovskite quantum-dot-sensitized solar cell, Nanoscale. 3 (2011) 4088–4093. doi:10.1039/c1nr10867k.

[26] M.M. Lee, J. Teuscher, T. Miyasaka, T.N. Murakami, H.J. Snaith, Efficient hybrid solar cells based on meso-superstructured organometal halide perovskites, Science. 338 (2012) 643–647. doi:10.1126/science.1228604.

[27] J.M. Ball, M.M. Lee, A. Hey, H.J. Snaith, Low-temperature processed meso-superstructured to thin-film perovskite solar cells, Energy Environ. Sci. 6 (2013) 1739–1743. doi:10.1039/C3EE40810H.

[28] J. Burschka, N. Pellet, S.-J. Moon, R. Humphry-Baker, P. Gao, M.K. Nazeeruddin, M. Grätzel, Sequential deposition as a route to high-performance perovskite-sensitized solar cells, Nature. 499 (2013) 316–319. doi:10.1038/nature12340.

[29] M. Liu, M.B. Johnston, H.J. Snaith, Efficient planar heterojunction perovskite solar cells by vapour deposition, Nature. 501 (2013) 395–398. doi:10.1038/nature12509.

[30] N.J. Jeon, H.G. Lee, Y.C. Kim, J. Seo, J.H. Noh, J. Lee, S.I. Seok, o-Methoxy substituents in spiro-OMeTAD for efficient inorganic-organic hybrid perovskite solar cells, J. Am. Chem. Soc. 136 (2014) 7837–7840. doi:10.1021/ja502824c.

[31] J.P.C. Baena, L. Steier, W. Tress, M. Saliba, S. Neutzner, T. Matsui, F. Giordano, T.J. Jacobsson, A.R.S. Kandada, S.M. Zakeeruddin, A. Petrozza, A. Abate, M.K. Nazeeruddin, M. Grätzel, A. Hagfeldt, Highly efficient planar perovskite solar cells through band alignment engineering, Energy Environ. Sci. 8 (2015) 2928–2934. doi:10.1039/C5EE02608C.

[32] H. Zhou, Q. Chen, G. Li, S. Luo, T. Song, H.-S. Duan, Z. Hong, J. You, Y. Liu, Y. Yang, Photovoltaics. Interface engineering of highly efficient perovskite solar cells, Science.

345 (2014) 542–546. doi:10.1126/science.1254050.

[33] W.S. Yang, J.H. Noh, N.J. Jeon, Y.C. Kim, S. Ryu, J. Seo, S.I. Seok, SOLAR CELLS. High-performance photovoltaic perovskite layers fabricated through intramolecular exchange, Science. 348 (2015) 1234–1237. doi:10.1126/science.aaa9272.

[34] E.H. Anaraki, A. Kermanpur, L. Steier, K. Domanski, T. Matsui, W. Tress, M. Saliba, A. Abate, M. Grätzel, A. Hagfeldt, J.-P. Correa-Baena, Highly efficient and stable planar perovskite solar cells by solution-processed tin oxide, Energy Environ. Sci. 9 (2016) 3128–3134. doi:10.1039/C6EE02390H.

[35] M. Saliba, T. Matsui, K. Domanski, J.-Y. Seo, A. Ummadisingu, S.M. Zakeeruddin, J.-P. Correa-Baena, W.R. Tress, A. Abate, A. Hagfeldt, M. Grätzel, Incorporation of rubidium cations into perovskite solar cells improves photovoltaic performance, Science. 354 (2016) 206–209. doi:10.1126/science.aah5557.

[36] Photovoltaic Research | NREL, (n.d.). https://www.nrel.gov/pv/ (accessed October 15, 2018).

[37] F.U. Hamelmann, Transparent Conductive Oxides in Thin Film Photovoltaics, J. Phys. Conf. Ser. 559 (2014) 012016. doi:10.1088/1742-6596/559/1/012016.

[38] M. Ye, X. Hong, F. Zhang, X. Liu, Recent advancements in perovskite solar cells: flexibility, stability and large scale, J. Mater. Chem. A. 4 (2016) 6755–6771. doi:10.1039/C5TA09661H.

[39] L. Qiu, J. Deng, X. Lu, Z. Yang, H. Peng, Integrating Perovskite Solar Cells into a Flexible Fiber, Angew. Chem. Int. Ed. 53 (2014) 10425–10428. doi:10.1002/anie.201404973.

[40] M. Lee, Y. Ko, Y. Jun, Efficient fiber-shaped perovskite photovoltaics using silver nanowires as top electrode, J. Mater. Chem. A. 3 (2015) 19310–19313. doi:10.1039/C5TA02779A.

[41] M.J. Uddin, T. Dickens, J. Yan, R. Chirayath, D.O. Olawale, O.I. Okoli, Solid state dye-sensitized photovoltaic micro-wires (DSPMs) with carbon nanotubes yarns as counter electrode: Synthesis and characterization, Sol. Energy Mater. Sol. Cells. 108 (2013) 65–69. doi:10.1016/j.solmat.2012.09.003.

[42] J. Yan, M.J. Uddin, T.J. Dickens, D.E. Daramola, O.I. Okoli, 3D Wire-Shaped Dye-Sensitized Solar Cells in Solid State Using Carbon Nanotube Yarns with Hybrid Photovoltaic Structure, Adv. Mater. Interfaces. 1 (2014) 1400075. doi:10.1002/admi.201400075.

[43] M.J. Uddin, D.E. Daramola, E. Velasquez, T.J. Dickens, J. Yan, E. Hammel, F. Cesano, O.I. Okoli, A high efficiency 3D photovoltaic microwire with carbon nanotubes (CNT)-quantum dot (QD) hybrid interface, Phys. Status Solidi RRL – Rapid Res. Lett. 8 (2014)

898–903. doi:10.1002/pssr.201409392.

[44] N. Marinova, S. Valero, J.L. Delgado, Organic and perovskite solar cells: Working principles, materials and interfaces, J. Colloid Interface Sci. 488 (2017) 373–389. doi:10.1016/j.jcis.2016.11.021.

[45] K. Feron, W.J. Belcher, C.J. Fell, P.C. Dastoor, Organic Solar Cells: Understanding the Role of Förster Resonance Energy Transfer, Int. J. Mol. Sci. 13 (2012) 17019–17047. doi:10.3390/ijms131217019.

[46] M.I. Asghar, J. Zhang, H. Wang, P.D. Lund, Device stability of perovskite solar cells – A review, Renew. Sustain. Energy Rev. 77 (2017) 131–146. doi:10.1016/j.rser.2017.04.003.

[47] Solar Cells: A Guide to Theory and Measurement, Ossila. (n.d.). https://www.ossila.com/pages/solar-cells-theory (accessed October 23, 2018).

[48] M. Habibi, F. Zabihi, M.R. Ahmadian-Yazdi, M. Eslamian, Progress in emerging solution-processed thin film solar cells – Part II: Perovskite solar cells, Renew. Sustain. Energy Rev. 62 (2016) 1012–1031. doi:10.1016/j.rser.2016.05.042.

[49] N.-G. Park, Perovskite solar cells: an emerging photovoltaic technology, Mater. Today. 18 (2015) 65–72. doi:10.1016/j.mattod.2014.07.007.

[50] V.M. Goldschmidt, Die Gesetze der Krystallochemie, Naturwissenschaften. 14 (1926) 477–485. doi:10.1007/BF01507527.

[51] M.A. Green, A. Ho-Baillie, H.J. Snaith, The emergence of perovskite solar cells, Nat. Photonics. 8 (2014) 506–514. doi:10.1038/nphoton.2014.134.

[52] Z. Song, S.C. Watthage, A.B. Phillips, M.J. Heben, Pathways toward high-performance perovskite solar cells: review of recent advances in organo-metal halide perovskites for photovoltaic applications, J. Photonics Energy. 6 (2016) 022001–022001. doi:10.1117/1.JPE.6.022001.

[53] J.-H. Im, H.-S. Kim, N.-G. Park, Morphology-photovoltaic property correlation in perovskite solar cells: One-step versus two-step deposition of CH3NH3PbI3, APL Mater. 2 (2014) 081510. doi:10.1063/1.4891275.

[54] J. Wei, Y. Zhao, H. Li, G. Li, J. Pan, D. Xu, Q. Zhao, D. Yu, Hysteresis Analysis Based on the Ferroelectric Effect in Hybrid Perovskite Solar Cells, (2014). doi:10.1021/jz502111u.

[55] H.-S. Kim, I.-H. Jang, N. Ahn, M. Choi, A. Guerrero, J. Bisquert, N.-G. Park, Control of I–V Hysteresis in CH3NH3PbI3 Perovskite Solar Cell, (2015). doi:10.1021/acs.jpclett.5b02273.

[56] B. Chen, M. Yang, S. Priya, K. Zhu, Origin of J–V Hysteresis in Perovskite Solar Cells, (2016). doi:10.1021/acs.jpclett.6b00215.

[57] Materials | Free Full-Text | Perovskites-Based Solar Cells: A Review of Recent Progress, Materials and Processing Methods, (n.d.). https://www.mdpi.com/1996-1944/11/5/729 (accessed October 16, 2018).

[58] J. You, L. Meng, T.-B. Song, T.-F. Guo, Y.M. Yang, W.-H. Chang, Z. Hong, H. Chen, H. Zhou, Q. Chen, Y. Liu, N. De Marco, Y. Yang, Improved air stability of perovskite solar cells via solution-processed metal oxide transport layers, Nat. Nanotechnol. 11 (2016) 75–81. doi:10.1038/nnano.2015.230.

[59] J.-Y. Jeng, Y.-F. Chiang, M.-H. Lee, S.-R. Peng, T.-F. Guo, P. Chen, T.-C. Wen, CH3NH3PbI3 Perovskite/Fullerene Planar-Heterojunction Hybrid Solar Cells, Adv. Mater. 25 (2013) 3727–3732. doi:10.1002/adma.201301327.

[60] D. Liu, J. Yang, T.L. Kelly, Compact Layer Free Perovskite Solar Cells with 13.5% Efficiency, J. Am. Chem. Soc. 136 (2014) 17116–17122. doi:10.1021/ja508758k.

[61] W. Ke, G. Fang, J. Wan, H. Tao, Q. Liu, L. Xiong, P. Qin, J. Wang, H. Lei, G. Yang, M. Qin, X. Zhao, Y. Yan, Efficient hole-blocking layer-free planar halide perovskite thin-film solar cells, Nat. Commun. 6 (2015) ncomms7700. doi:10.1038/ncomms7700.

[62] L. Etgar, P. Gao, Z. Xue, Q. Peng, A.K. Chandiran, B. Liu, M.K. Nazeeruddin, M. Grätzel, Mesoscopic CH3NH3PbI3/TiO2 Heterojunction Solar Cells, J. Am. Chem. Soc. 134 (2012) 17396–17399. doi:10.1021/ja307789s.

[63] S. Aharon, S. Gamliel, B.E. Cohen, L. Etgar, Depletion region effect of highly efficient hole conductor free CH3NH3PbI3 perovskite solar cells, Phys. Chem. Chem. Phys. 16 (2014) 10512–10518. doi:10.1039/C4CP00460D.

[64] W.-Q. Wu, Q. Wang, Y. Fang, Y. Shao, S. Tang, Y. Deng, H. Lu, Y. Liu, T. Li, Z. Yang, A. Gruverman, J. Huang, Molecular doping enabled scalable blading of efficient hole-transport-layer-free perovskite solar cells, Nat. Commun. 9 (2018) 1625. doi:10.1038/s41467-018-04028-8.

[65] Y. Liu, S. Ji, S. Li, W. He, K. Wang, H. Hu, C. Ye, Study on hole-transport-material-free planar TiO2/CH3NH3PbI3 heterojunction solar cells: the simplest configuration of a working perovskite solar cell, J. Mater. Chem. A. 3 (2015) 14902–14909. doi:10.1039/C5TA03693C.

[66] W.-J. Yin, J.-H. Yang, J. Kang, Y. Yan, S.-H. Wei, Halide perovskite materials for solar cells: a theoretical review, J. Mater. Chem. A. 3 (2015) 8926–8942. doi:10.1039/C4TA05033A.

[67] L. Huang, J. Xu, X. Sun, Y. Du, H. Cai, J. Ni, J. Li, Z. Hu, J. Zhang, Toward Revealing the Critical Role of Perovskite Coverage in Highly Efficient Electron-Transport Layer-Free Perovskite Solar Cells: An Energy Band and Equivalent Circuit Model Perspective, ACS Appl. Mater. Interfaces. 8 (2016) 9811–9820. doi:10.1021/acsami.6b00544.

[68] J.-P. Correa-Baena, A. Abate, M. Saliba, W. Tress, T.J. Jacobsson, M. Grätzel, A. Hagfeldt, The rapid evolution of highly efficient perovskite solar cells, Energy Environ. Sci. 10 (2017) 710–727. doi:10.1039/C6EE03397K.

[69] F.C. Hanusch, E. Wiesenmayer, E. Mankel, A. Binek, P. Angloher, C. Fraunhofer, N. Giesbrecht, J.M. Feckl, W. Jaegermann, D. Johrendt, T. Bein, P. Docampo, Efficient Planar Heterojunction Perovskite Solar Cells Based on Formamidinium Lead Bromide, J. Phys. Chem. Lett. 5 (2014) 2791–2795. doi:10.1021/jz501237m.

[70] M. Saliba, T. Matsui, J.-Y. Seo, K. Domanski, J.-P. Correa-Baena, M. Khaja Nazeeruddin, S. M. Zakeeruddin, W. Tress, A. Abate, A. Hagfeldt, M. Grätzel, Cesium-containing triple cation perovskite solar cells: improved stability, reproducibility and high efficiency, Energy Environ. Sci. 9 (2016) 1989–1997. doi:10.1039/C5EE03874J.

[71] H. Choi, J. Jeong, H.-B. Kim, S. Kim, B. Walker, G.-H. Kim, J.Y. Kim, Cesium-doped methylammonium lead iodide perovskite light absorber for hybrid solar cells, Nano Energy. 7 (2014) 80–85. doi:10.1016/j.nanoen.2014.04.017.

[72] J.-W. Lee, D.-H. Kim, H.-S. Kim, S.-W. Seo, S.M. Cho, N.-G. Park, Formamidinium and Cesium Hybridization for Photo- and Moisture-Stable Perovskite Solar Cell, Adv. Energy Mater. 5 (2015) 1501310. doi:10.1002/aenm.201501310.

[73] J.H. Noh, S.H. Im, J.H. Heo, T.N. Mandal, S.I. Seok, Chemical management for colorful, efficient, and stable inorganic-organic hybrid nanostructured solar cells, Nano Lett. 13 (2013) 1764–1769. doi:10.1021/nl400349b.

[74] W.-Q. Wu, D. Chen, R.A. Caruso, Y.-B. Cheng, Recent progress in hybrid perovskite solar cells based on n-type materials, J. Mater. Chem. A. 5 (2017) 10092–10109. doi:10.1039/C7TA02376F.

[75] H.-H. Wang, Q. Chen, H. Zhou, L. Song, Z.S. Louis, N.D. Marco, Y. Fang, P. Sun, T.-B. Song, H. Chen, Y. Yang, Improving the TiO2 electron transport layer in perovskite solar cells using acetylacetonate-based additives, J. Mater. Chem. A. 3 (2015) 9108–9115. doi:10.1039/C4TA06394E.

[76] Q. Jiang, X. Zhang, J. You, SnO2: A Wonderful Electron Transport Layer for Perovskite Solar Cells, Small. 14 (2018) 1801154. doi:10.1002/smll.201801154.

[77] Q. An, P. Fassl, Y.J. Hofstetter, D. Becker-Koch, A. Bausch, P.E. Hopkinson, Y. Vaynzof, High performance planar perovskite solar cells by ZnO electron transport layer

engineering, Nano Energy. 39 (2017) 400–408. doi:10.1016/j.nanoen.2017.07.013.

[78] S. Yoon, S.J. Kim, H.S. Kim, J.-S. Park, I.K. Han, J.W. Jung, M. Park, Solution-processed indium oxide electron transporting layers for high-performance and photo-stable perovskite and organic solar cells, Nanoscale. 9 (2017) 16305–16312. doi:10.1039/C7NR05695H.

[79] K. Wang, Y. Shi, Q. Dong, Y. Li, S. Wang, X. Yu, M. Wu, T. Ma, Low-Temperature and Solution-Processed Amorphous WOX as Electron-Selective Layer for Perovskite Solar Cells, J. Phys. Chem. Lett. 6 (2015) 755–759. doi:10.1021/acs.jpclett.5b00010.

[80] X. Wang, L.-L. Deng, L.-Y. Wang, S.-M. Dai, Z. Xing, X.-X. Zhan, X.-Z. Lu, S.-Y. Xie, R.-B. Huang, L.-S. Zheng, Cerium oxide standing out as an electron transport layer for efficient and stable perovskite solar cells processed at low temperature, J. Mater. Chem. A. 5 (2017) 1706–1712. doi:10.1039/C6TA07541J.

[81] M.F.M. Noh, C.H. Teh, R. Daik, E.L. Lim, C.C. Yap, M.A. Ibrahim, N.A. Ludin, A.R. bin M. Yusoff, J. Jang, M.A.M. Teridi, The architecture of the electron transport layer for a perovskite solar cell, J. Mater. Chem. C. 6 (2018) 682–712. doi:10.1039/C7TC04649A.

[82] Q. Zhang, C.S. Dandeneau, X. Zhou, G. Cao, ZnO Nanostructures for Dye-Sensitized Solar Cells, Adv. Mater. 21 (2009) 4087–4108. doi:10.1002/adma.200803827.

[83] X. Dong, H. Hu, B. Lin, J. Ding, N. Yuan, The effect of ALD-Zno layers on the formation of CH3NH3PbI3 with different perovskite precursors and sintering temperatures, Chem. Commun. 50 (2014) 14405–14408. doi:10.1039/C4CC04685D.

[84] K. Mahmood, S. Sarwar, M.T. Mehran, Current status of electron transport layers in perovskite solar cells: materials and properties, RSC Adv. 7 (2017) 17044–17062. doi:10.1039/C7RA00002B.

[85] S. Pitchaiya, M. Natarajan, A. Santhanam, V. Asokan, A. Yuvapragasam, V. Madurai Ramakrishnan, S.E. Palanisamy, S. Sundaram, D. Velauthapillai, A review on the classification of organic/inorganic/carbonaceous hole transporting materials for perovskite solar cell application, Arab. J. Chem. (2018). doi:10.1016/j.arabjc.2018.06.006.

[86] Z. Yu, L. Sun, Recent Progress on Hole-Transporting Materials for Emerging Organometal Halide Perovskite Solar Cells, Adv. Energy Mater. 5 (2015) 1500213. doi:10.1002/aenm.201500213.

[87] Z.H. Bakr, Q. Wali, A. Fakharuddin, L. Schmidt-Mende, T.M. Brown, R. Jose, Advances in hole transport materials engineering for stable and efficient perovskite solar cells, Nano Energy. 34 (2017) 271–305. doi:10.1016/j.nanoen.2017.02.025.

[88] H. Xi, S. Tang, X. Ma, J. Chang, D. Chen, Z. Lin, P. Zhong, H. Wang, C. Zhang, Performance Enhancement of Planar Heterojunction Perovskite Solar Cells through Tuning the Doping Properties of Hole-Transporting Materials, ACS Omega. 2 (2017) 326–336. doi:10.1021/acsomega.6b00465.

[89] D. Bi, L. Yang, G. Boschloo, A. Hagfeldt, E.M.J. Johansson, Effect of Different Hole Transport Materials on Recombination in CH3NH3PbI3 Perovskite-Sensitized Mesoscopic Solar Cells, J. Phys. Chem. Lett. 4 (2013) 1532–1536. doi:10.1021/jz400638x.

[90] H.A. Abbas, R. Kottokkaran, B. Ganapathy, M. Samiee, L. Zhang, A. Kitahara, M. Noack, V.L. Dalal, High efficiency sequentially vapor grown n-i-p CH3NH3PbI3 perovskite solar cells with undoped P3HT as p-type heterojunction layer, APL Mater. 3 (2015) 016105. doi:10.1063/1.4905932.

[91] Y. Xiao, G. Han, Y. Chang, H. Zhou, M. Li, Y. Li, An all-solid-state perovskite-sensitized solar cell based on the dual function polyaniline as the sensitizer and p-type hole-transporting material, J. Power Sources. 267 (2014) 1–8. doi:10.1016/j.jpowsour.2014.05.053.

[92] Z. Hawash, L.K. Ono, Y. Qi, Recent Advances in Spiro-MeOTAD Hole Transport Material and Its Applications in Organic–Inorganic Halide Perovskite Solar Cells, Adv. Mater. Interfaces. 5 (2018) 1700623. doi:10.1002/admi.201700623.

[93] J.A. Christians, R.C.M. Fung, P.V. Kamat, An inorganic hole conductor for organo-lead halide perovskite solar cells. Improved hole conductivity with copper iodide, J. Am. Chem. Soc. 136 (2014) 758–764. doi:10.1021/ja411014k.

[94] K.-C. Wang, P.-S. Shen, M.-H. Li, S. Chen, M.-W. Lin, P. Chen, T.-F. Guo, Low-temperature sputtered nickel oxide compact thin film as effective electron blocking layer for mesoscopic NiO/CH3NH3PbI3 perovskite heterojunction solar cells, ACS Appl. Mater. Interfaces. 6 (2014) 11851–11858. doi:10.1021/am503610u.

[95] P. Qin, S. Tanaka, S. Ito, N. Tetreault, K. Manabe, H. Nishino, M.K. Nazeeruddin, M. Grätzel, Inorganic hole conductor-based lead halide perovskite solar cells with 12.4% conversion efficiency, Nat. Commun. 5 (2014) 3834. doi:10.1038/ncomms4834.

[96] M. Peng, D. Zou, Flexible fiber/wire-shaped solar cells in progress: properties, materials, and designs, J. Mater. Chem. A. 3 (2015) 20435–20458. doi:10.1039/C5TA03731J.

[97] H. Hu, K. Yan, M. Peng, X. Yu, S. Chen, B. Chen, B. Dong, X. Gao, D. Zou, Fiber-shaped perovskite solar cells with 5.3% efficiency, J. Mater. Chem. A. 4 (2016) 3901–3906. doi:10.1039/C5TA09280A.

[98] X. Wang, S.A. Kulkarni, Z. Li, W. Xu, S.K. Batabyal, S. Zhang, A. Cao, L.H. Wong, Wire-shaped perovskite solar cell based on TiO2 nanotubes, Nanotechnology. 27 (2016)

20LT01. doi:10.1088/0957-4484/27/20/20LT01.

[99] J. Deng, L. Qiu, X. Lu, Z. Yang, G. Guan, Z. Zhang, H. Peng, Elastic perovskite solar cells, J. Mater. Chem. A. 3 (2015) 21070–21076. doi:10.1039/C5TA06156C.

[100] S. Iijima, Helical microtubules of graphitic carbon, Nature. 354 (1991) 56–58. doi:10.1038/354056a0.

[101] R.H. Baughman, A.A. Zakhidov, W.A. de Heer, Carbon Nanotubes--the Route Toward Applications, Science. 297 (2002) 787–792. doi:10.1126/science.1060928.

[102] J.M. Lee, C. Choi, J.H. Kim, M.J. de Andrade, R.H. Baughman, S.J. Kim, Biscrolled Carbon Nanotube Yarn Structured Silver-Zinc Battery, Sci. Rep. 8 (2018) 11150. doi:10.1038/s41598-018-29266-0.

[103] T. Chen, L. Dai, Carbon nanomaterials for high-performance supercapacitors, Mater. Today. 16 (2013) 272–280. doi:10.1016/j.mattod.2013.07.002.

[104] I.V. Zaporotskova, N.P. Boroznina, Y.N. Parkhomenko, L.V. Kozhitov, Carbon nanotubes: Sensor properties. A review, Mod. Electron. Mater. 2 (2016) 95–105. doi:10.1016/j.moem.2017.02.002.

[105] C. Li, E.T. Thostenson, T.-W. Chou, Sensors and actuators based on carbon nanotubes and their composites: A review, Compos. Sci. Technol. 68 (2008) 1227–1249. doi:10.1016/j.compscitech.2008.01.006.

[106] A. Bianco, K. Kostarelos, M. Prato, Applications of carbon nanotubes in drug delivery, Curr. Opin. Chem. Biol. 9 (2005) 674–679. doi:10.1016/j.cbpa.2005.10.005.

[107] M. Notarianni, J. Liu, K. Vernon, N. Motta, Synthesis and applications of carbon nanomaterials for energy generation and storage, Beilstein J. Nanotechnol. 7 (2016) 149–196. doi:10.3762/bjnano.7.17.

[108] M.F.L.D. Volder, S.H. Tawfick, R.H. Baughman, A.J. Hart, Carbon Nanotubes: Present and Future Commercial Applications, Science. 339 (2013) 535–539. doi:10.1126/science.1222453.

[109] A. Aqel, K.M.M.A. El-Nour, R.A.A. Ammar, A. Al-Warthan, Carbon nanotubes, science and technology part (I) structure, synthesis and characterisation, Arab. J. Chem. 5 (2012) 1–23. doi:10.1016/j.arabjc.2010.08.022.

[110] L. Wei, N. Tezuka, T. Umeyama, H. Imahori, Y. Chen, Formation of single-walled carbon nanotube thin films enriched with semiconducting nanotubes and their application in photoelectrochemical devices, Nanoscale. 3 (2011) 1845–1849. doi:10.1039/c0nr00986e.

[111] J. Yan, M.J. Uddin, T.J. Dickens, O.I. Okoli, Carbon nanotubes (CNTs) enrich the solar cells, Sol. Energy. 96 (2013) 239–252. doi:10.1016/j.solener.2013.07.027.

[112] T. Chen, L. Qiu, Z. Cai, F. Gong, Z. Yang, Z. Wang, H. Peng, Intertwined Aligned Carbon Nanotube Fiber Based Dye-Sensitized Solar Cells, Nano Lett. 12 (2012) 2568–2572. doi:10.1021/nl300799d.

[113] D. Yang, R. Yang, J. Zhang, Z. Yang, S. (Frank) Liu, C. Li, High efficiency flexible perovskite solar cells using superior low temperature TiO2, Energy Environ. Sci. 8 (2015) 3208–3214. doi:10.1039/C5EE02155C.

[114] N. Ahn, D.-Y. Son, I.-H. Jang, S.M. Kang, M. Choi, N.-G. Park, Highly Reproducible Perovskite Solar Cells with Average Efficiency of 18.3% and Best Efficiency of 19.7% Fabricated via Lewis Base Adduct of Lead(II) Iodide, J. Am. Chem. Soc. 137 (2015) 8696–8699. doi:10.1021/jacs.5b04930.

[115] J.-H. Im, I.-H. Jang, N. Pellet, M. Grätzel, N.-G. Park, Growth of $CH_3NH_3PbI_3$ cuboids with controlled size for high-efficiency perovskite solar cells, Nat. Nanotechnol. 9 (2014) 927–932. doi:10.1038/nnano.2014.181.

[116] G. Grissom, J. Jaksik, M. McEntee, E.M. Durke, S.T.J. Aishee, M. Cua, O. Okoli, A. Touhami, H.J. Moore, M.J. Uddin, Three-dimensional carbon nanotube yarn based solid state solar cells with multiple sensitizers exhibit high energy conversion efficiency, Sol. Energy. 171 (2018) 16–22. doi:10.1016/j.solener.2018.06.053.

[117] J.-F. Wang, L. Zhu, B.-G. Zhao, Y.-L. Zhao, J. Song, X.-Q. Gu, Y.-H. Qiang, Surface engineering of perovskite films for efficient solar cells, Sci. Rep. 7 (2017) 14478. doi:10.1038/s41598-017-14920-w.

BIOGRAPHICAL SKETCH

Istiak Hussain started his Master's program in Chemistry at the University of Texas Rio Grande Valley in 2017. He received his Bachelor of Science degree from University of Science and Technology in 2016. He worked as a research assistant at the Photonics and Energy Research lab under Dr. Mohammed Uddin during his Master's studies. He also worked as a teaching assistant at the department of chemistry. He received his Masters of Science degree in Chemistry in December of 2018. He can be reached at hussain.istiak@gmail.com.